Chemotactic motility and biofilm formation in *Campylobacter jejuni* are coordinated by the CheAYWVX system

Mark Reuter[1,*], Eveline Ultee[1], Yasmin Toseafa[1], Andrew Tan[1], and Arnoud H.M. van Vliet[1,2,*]

1. Quadram Institute, Gut Health and Food Safety Programme, Norwich Research Park, Norwich, United Kingdom.
2. University of Surrey, Department of Pathology and Infectious Diseases, School of Veterinary Medicine, Faculty of Health and Medical Sciences, Guildford, United Kingdom

Running title: Chemotaxis and biofilm formation in *C. jejuni*

* Address correspondence to Dr Mark Reuter (mark.reuter@googlemail.com) or Dr Arnoud van Vliet (a.vanvliet@surrey.ac.uk)

Total number of words in Summary: 297

Total number of words in Manuscript text: 5876

Number of Figures: 8

Number of Tables: 2

Supplementary information: 6 Figures, 2 Movies, 1 Table

ABSTRACT

Chemotaxis is the ability of motile bacteria to coordinate swimming behaviour to navigate a changeable environment, an important and rapid adaptative response directing cells to either move away from repellent stimuli or to move towards more favourable conditions using chemical gradients sensed by receptors in the bacterial membrane. In the foodborne bacterial pathogen *Campylobacter jejuni*, flagellar motility and chemotaxis are required for intestinal colonisation and virulence, and may also play a role in environmental survival via biofilm formation. Here we present a systematic characterisation of the CheAYVW chemotaxis system of *C. jejuni*, and its role in directed motility and biofilm formation. Inactivation of any of the core chemotaxis genes (*cheA*, *cheY*, *cheV* or *cheW*) impaired chemotactic motility but not flagellar assembly. Inactivation of *cheV* or presence of two copies of *cheV* impaired chemotaxis to a greater extent than inactivation of *cheW* or presence of two copies of *cheW*. A *cheY* mutant swam in clockwise loops and this behaviour was ameliorated by complementation with wildtype *cheY* or a *cheY* gene lacking the conserved phosphorylation site, but not by complementation with *cheY* lacking the metal-binding site. Although the *C. jejuni* CheA protein contains a CheY-like domain, deletion of this CheY-like domain from CheA did not impair chemotactic motility, nor could it complement a *cheY* mutant. Next to the core *cheAYVW* chemotaxis genes, we also investigated the role of the putative *cheX* gene *cj0350*. The presence of two copies of *cheX* resulted in reduced chemotactic motility. Finally, inactivation of any of the core chemotaxis genes interfered with the ability to form a distinct biofilm at an air-media interface. In conclusion, the *Campylobacter* chemotaxis system has specific components making it distinct from the *E. coli* and *B. subtilis* model organisms, requiring specific assessment of their roles in the biology of *Campylobacter*.

45 **INTRODUCTION**

46 *Campylobacter jejuni* is an important causative agent of bacterial gastroenteritis in humans [1],
47 and is commonly transmitted via contaminated food, especially poultry meat [2]. Infection with *C.*
48 *jejuni* is also associated with neurodegenerative diseases like Miller-Fisher and Guillain-Barre
49 syndrome [3]. One of the key factors for infection by *C. jejuni* is its flagella-based motility, as
50 aflagellated *C. jejuni* are unable to cause disease in animal models and show strongly reduced host
51 cell invasion in cell culture-based assays [4-6]. The flagella are also involved in biofilm formation
52 [7-9], and are targeted by bacteriophages [10].

53 Bacteria are able to adapt to changeable environments using a number of different strategies.
54 Over time, genome plasticity and evolution allows for long-term adaptation to a particular niche.
55 More immediate stresses are directly/indirectly sensed by transcriptional regulators, resulting in
56 changes in gene expression. By far the most rapid means of evading stress by motile bacteria, is by
57 changing swimming behaviour to escape unfavourable conditions or seek more favourable
58 conditions, using chemotaxis [11, 12]. The core chemotaxis pathway has been extensively
59 characterised in model organisms such as *E. coli* and *B. subtilis*, and consists of the CheYA two-
60 component signal transduction system [13, 14]. Stimulation of signal sensing methyl-accepting
61 chemotaxis proteins (MCPs) results in autophosphorylation of the histidine kinase CheA, which
62 transfers the phosphate group to the response regulator CheY. Phospho-CheY interacts with the
63 flagellar switch to alter rotation. Counter-clockwise rotation commonly results in straight darting
64 motility while clockwise rotation results in a tumbling behaviour and directional change [15].

65 While the core CheA-CheY pathway is conserved in motile bacteria, the bacterial kingdom
66 contains several variations on this theme [16]. For instance, phosphorylation of CheY results in
67 clockwise flagella rotation in *E. coli* [17, 18], while in *B. subtilis*, the inability to phosphorylate
68 CheY results in clockwise rotation and tumbling motility [19, 20]. Furthermore, a number of
69 accessory proteins are involved, such as the CheW protein which is required for CheA-MCP

70 interaction [21, 22], while a methyltransferase (CheR) and a methylesterase (CheB) modify the
71 MCP proteins to accommodate adaptation [23]. Some organisms contain the CheW-like protein
72 CheV, which may help integrate signals from a specific class of sensors and may also act as a
73 phosphate sink [24]. There are also bacteria which have multiple non-redundant homologs of the
74 chemotaxis proteins or contain specific adaptations, adjuncts, and domain-fusions that add new
75 functions to the core chemotaxis system [25, 26].

76 Compared to other foodborne pathogens such as *E. coli*, *Salmonella*, and *Listeria*, *C. jejuni* has
77 a greater number of MCPs involved in sensing amino acids, deoxycholate, dicarboxylic acid TCA
78 intermediates, formic acid, fucose, redox and energy status [27-35], plus a core chemotaxis system
79 consisting of CheA-Y-W-V proteins plus a CheR and a truncated CheB protein [36]. Chemotaxis-
80 defective mutants have been shown to be attenuated in disease models [28, 37-39], show reduced
81 immunopathology [40] and chick colonization [39, 41], and were reported to be crucial for infection
82 in genome-wide transposon mutant screenings for virulence factors [42, 43].

83 In this manuscript we have systematically examined the core chemotaxis pathway in *C. jejuni*
84 (Fig 1). We show that each signalling protein is necessary for robust chemotaxis in complex media,
85 but not for motility. Both CheW and CheV adaptor proteins are required for chemotaxis, but they
86 have distinct functions. Furthermore, we show that the CheY protein requires a metal-binding site
87 but not necessarily the predicted site of phosphorylation, suggesting a possible phosphorylation-
88 independent interaction with the flagella switch. We show that the receiver domain of CheA (CheA-
89 Y) is dispensable for CheA function, but cannot complement a *cheY* mutant. We further identify a
90 putative ortholog of the CheX phosphatase, which attenuates chemotaxis when present in multiple
91 copies, and that chemotaxis is required for organized biofilm formation.

92

93 **MATERIALS AND METHODS**

94

95 ***C. jejuni* strains and growth conditions.**

96 *Campylobacter jejuni* strain NCTC 11168 and its isogenic mutants (Table 1) were routinely
97 cultured in a MACS-MG-1000 controlled atmosphere cabinet (Don Whitley Scientific) under
98 microaerobic conditions (85% N_2, 5% O_2, 10% CO_2) at 37°C. For growth on plates, strains were
99 either grown on Brucella agar or Blood Agar Base (BAB) with Skirrow supplement (10 μg ml^{-1}
100 vancomycin, 5 μg ml^{-1} trimethoprim, 2.5 IU polymyxin-B). Broth culture was carried out in
101 Brucella broth (Becton Dickinson).

102

103 **Construction of insertional inactivation strains**

104 Plasmids used in this study are listed in Table 2. Insertional inactivation mutants were made as
105 described previously [33] using primers listed in Table S1. To insert antibiotic resistance cassettes,
106 *Bam*HI sites were introduced in the target genes by inverse PCR (Table S1) and ligated to either the
107 kanamycin cassette from pMARKan9 (*ΔcheY*, Δ*cheW*, Δ*cheV*) or chloramphenicol cassette from
108 pTopCat. All constructs were sequenced prior to transformation (Eurofins Genomics, Ebersberg,
109 Germany). Single *C. jejuni* mutant strains were isolated after transformation of the *C. jejuni* NCTC
110 11168 wild-type strain with plasmids by electroporation [33], followed by selection on plates
111 supplemented with either 50 μg ml^{-1} kanamycin or 10 μg ml^{-1} chloramphenicol. To confirm the
112 position of the antibiotic cassette in antibiotic resistant clones, genomic DNA was isolated from
113 four ml of overnight culture (DNeasy kit, QIAGEN). Diluted genomic DNA (50 ng) was used as
114 template for PCR using primers that anneal outside of the cloned flanking regions in combination
115 with antibiotic cassette-specific primers (Table S1).

116

117 **Construction of complementation constructs and site directed mutagenesis**

118 *C. jejuni* mutants were complemented by inserting the individual chemotaxis genes (*cheA*,
119 *cheY*, *cheW*, *cheV*, *cheAY*, *cj0350, fliN*) *in trans* using the *cj0046* pseudogene, as described

120 previously [33]. To make the CheY^{D53A} substitution, pCASO59 was used as template for inverse
121 PCR using primers CheYDA01/02 (Table S1). To make the CheY^{D7A} substitution, pCASO59 was
122 used as template for inverse PCR using primers cheYD7AFwd/Rev (Table S1). To make the
123 CheAΔReceiver domain construct (CheA$^{\Delta Rec}$), pCASO58 was used as template for inverse PCR
124 using primers cheARec01/02, which changes the codon encoding lysine 648 to a stop codon (see
125 Table S1). The inverse PCR products were digested with *Dpn*I for 60 minutes at 37°C and then
126 purified (PCR purification kit, QIAGEN) and transformed into *E. coli*. To identify clones
127 containing altered sequences, plasmid DNA was purified and sequenced using appropriate primers
128 (Eurofins Genomics, Ebersberg, Germany).
129

130 **RNA Extraction and RT-PCR**

131 RNA was extracted using the hot phenol method [44]. RNA concentration was determined
132 using a Nanodrop 2000 (Thermo Fisher Scientific). A mix of Moloney Murine Leukemia Virus (M-
133 MuLV) Reverse Transcriptase and murine RNase Inhibitor with an optimized random primer mix
134 was used to make cDNA (NEB). Two µg of RNA was mixed with random primers (6 µM final
135 concentration) and water and incubated at 70°C for 5 minutes then on ice for 5 minutes. This mix
136 was added to 10 µl of M-MuLV reaction mix and 2 µl M-MuLV enzyme mix in a total volume of
137 20 µl. Control reactions were also prepared containing 2 µl water in place of enzyme to show any
138 amplification from contaminating DNA. Reactions were incubated at 25°C for 5 minutes, 42°C for
139 60 minutes, then 80°C for 4 minutes. Reactions were made to total volume of 50 µl by adding 30 µl
140 water. For PCR, 2 µl of cDNA was mixed with OneTaq HotStart master mix (1× final
141 concentration, NEB), and gene-specific primers (0.2 µM final concentration) in a total volume of 25
142 µl. Extension reactions were carried out at 68°C.
143

144 **Assessment of growth**

145 A 50 µl single-use glycerol stock, routinely stored at -80°C, was used to inoculate a BAB plate
146 with Skirrow supplements and these cells were used to inoculate fresh Brucella broth. Cultures were
147 grown in microaerobic conditions with shaking overnight at 37°C. The overnight culture was
148 diluted to $A_{600} \approx 0.05$ (~ 1×10^7 CFU ml^{-1}) in 200 µl in a 96-well plate (flat bottom, non-treated,
149 sterile, polystyrene, (Corning, NY, USA)). Growth in 96-well plates was assessed using an Omega
150 plate reader (FLUOstar Omega (BMG Labtech, Germany)) linked to an atmospheric control unit in
151 microaerobic conditions at 37°C. Omega assays were run for 24 hours (double orbital shaking at
152 400 rpm) and A_{600} data was recorded every 60 minutes.

153

154 **Light microscopy and flagella staining using the Ryu stain**

155 Typically, 10 µl of an overnight culture was examined using an Eclipse 50i microscope (×100
156 lens) to monitor swimming phenotypes. When necessary, a Coolpix 4500 digital camera (Nikon)
157 was used to capture video (15 frames $second^{-1}$, 320×240 pixels). Video compilations were made by
158 extracting appropriate frames using ImageJ (Rasband, W.S., ImageJ, U. S. National Institutes of
159 Health, Bethesda, Maryland, USA, http://imagej.nih.gov/ij/, 1997-2014). To plot swimming
160 behaviour, individual cells were tracked using the Manual tracking plug-in for ImageJ (Fabrice
161 Cordeli, http://rsb.info.nih.gov/ij/plugins/track/track.html) then visualized using the Chemotaxis and
162 Migration Tool (Ibidi, http://ibidi.com/software/chemotaxis_and_migration_tool/). To visualise
163 flagella, cells were stained using the Ryu stain [45] as described previously [46]. ImageJ was used
164 to add a scale bar and prepare montage images.

165

166 **Chemotaxis assays**

167 Chemotactic motility was measured using soft agar motility assays and tube taxis assays [33].
168 All soft agar motility assays were carried out using square 10 mm^2 petri plates (Sterilin) inoculated

169 with wild-type and three test strains, as described previously [33]. For each plate, halo size was
170 expressed as a percentage of the corresponding wild-type and each strain was tested for significance
171 using a one-sample t-test (alpha = 0.05), compared to a hypothetical value of 100 (GraphPad Prism
172 6.01). Strain-to-strain comparisons were made using a two-tailed Mann-Whitney test.

173 Tube taxis assays were prepared as described previously [33]. The tubes were incubated at
174 37°C in air in a waterbath (Grant). Tubes were photographed after 24, 40, 48, 64, and 72 hours and
175 the dye front was measured from the top of the agar using the ImageJ software and expressed as a
176 percentage of the wild-type strain. Each strain was tested for significance using a one-sample t-test
177 (alpha = 0.05) compared to a hypothetical value of 100 (GraphPad Prism 6.01) and strain-to-strain
178 comparisons were made using a two-tailed Mann-Whitney test.

179

180 **Biofilm assays**

181 A 50 µl single-use glycerol stock, routinely stored at -80°C, was used to inoculate a BAB plate
182 with Skirrow supplements and these cells were used to inoculate fresh Brucella broth. Cultures were
183 grown in microaerobic conditions with shaking overnight at 37°C. The overnight culture was
184 diluted to $A_{600} \approx 0.05$ (~ 1 x 10^7 CFU ml^{-1}) in 22 ml sterile Brucella in a 50 ml flacon tube. A twin-
185 frost microscope slide (sterilized in 70% ethanol) was inserted into each falcon tube. Tubes were
186 incubated at 37°C in microaerobic conditions without shaking. After 48 hours, slides were removed
187 from the tubes using flamed-sterilized tweezers and briefly washed in water. Slides were dried in air
188 before staining with 1% crystal violet. Unbound crystal violet was washed off with water and slides
189 were dried in air. Biofilms were imaged using a GenePixPro microarray scanner (Axon). The
190 photomultiplier tube (PMT) gain of either the 635 nm or 532 nm laser was adjusted to achieve a
191 balanced image. To assess biofilm shedding, the A_{600} of the planktonic cultures were measured;
192 statistically different results were determined using a two-tailed Mann-Whitney test (GraphPad
193 Prism 6.01).

194

195 **Bioinformatic analysis.**

196 Pfam (http://pfam.sanger.ac.uk/ and InterProScan (http://www.ebi.ac.uk/Tools/pfa/iprscan/)
197 were used to search for protein domains and architectures. All BLAST searches were conducted
198 within BioEdit. EMBOSS Water was used for pairwise protein alignments
199 (http://www.ebi.ac.uk/Tools/psa/emboss_water/). ClustalX was used for multiple sequence
200 alignment (http://www.clustal.org/clustal2/). DeepView version 4.1 was used to make the CheY
201 model (http://spdbv.vital-it.ch/).

202

203 **RESULTS**

204

205 **CheV is the dominant adaptor protein in the chemotaxis signalling pathway**

206 In paradigm chemotaxis models, CheW has a role in stabilizing the CheA-MCP interaction [24,
207 47]. All *Campylobacter* genomes on the PATRIC database that contain a predicted *cheW* gene also
208 contain a predicted *cheV* gene. To assess the roles of CheW and CheV (which comprises a CheW
209 domain and C-terminal Receiver domain (Fig. 1)) in *C. jejuni*, each gene was inactivated by a
210 kanamycin cassette in the same orientation as the original gene. The *cheW* and *cheV* mutants grew
211 at the same rate as the wild-type strain (Fig. S1) and flagella were present at each pole of the cell
212 (Fig. 2). In liquid media, the swimming phenotype of the *cheW* and *cheV* mutants was comparable
213 to the wild-type. Chemotactic motility was assessed using soft agar motility plates and tube taxis,
214 which measures motility in both an energy and redox gradient [33]. Both halo formation and
215 migration were reduced compared to the wild-type. Chemotactic motility of the *cheW* mutant was
216 reduced to less than 50% compared to the wild-type strain at both 24 and 48 hours, respectively
217 (Fig. 3, 4). The reduction in halo formation and migration was more severe in the *cheV* mutant, as it
218 was reduced to less than one-third compared to the wild-type strain at both 24 and 48 hours (Fig. 3,

219 4). Thus, absence of CheV has a more dramatic effect on chemotaxis than absence of CheW in *C.*
220 *jejuni*. Introduction of the *cheW* mutant *in trans* in the *cj0046* pseudogene [33] resulted in the
221 complementation of the chemotaxis phenotypes of the *cheW* mutant (Fig. 3, 4). However,
222 complementation of the *cheV* mutant with *cheV* in the *cj0046* pseudogene did not restore
223 chemotactic motility. The *cheV* mutant still expressed the downstream *cheA* and *cheW* genes as
224 shown by reverse transcriptase PCR (Fig. S2A), suggesting the phenotype of the *cheV* mutant are
225 not due to polar effects on the transcription of the downstream *cheA* and *cheW* genes.
226 Supplementation of the wild-type strain with a second copy of *cheV* (WT +*cheV*) did not alter
227 swimming in liquid media, but led to a significant reduction in chemotactic motility (Fig. S3),
228 suggesting that the stoichiometry of CheV and other chemotaxis proteins is of importance for its
229 function. Finally, given that *C. jejuni* CheV contains an N-terminal CheW domain, the ability of
230 CheV to substitute for CheW was assessed by introducing the *cheV* gene into the *cheW* mutant. The
231 resulting *cheW* +*cheV* strain did not complement the *cheW* mutant (Fig. 3, 4).
232

233 **Increased levels of CheY augment chemotaxis**

234 The growth phenotype of a *cheY* mutant was not significantly different to the wild-type (Fig.
235 S1) and light microscopy revealed bi-polar flagella (Fig. 2). In liquid media, cells showed a
236 'Catherine Wheel' swimming behaviour [48], where a cell would appear to get trapped in a
237 clockwise swimming loop (see Movie 1 and Fig. 5B) before resuming a darting motility as observed
238 in the wild-type (Fig. 5A). The *cheY* mutant displayed the previously described chemotaxis defect
239 [38], with chemotactic motility reduced to less than 20% of wild-type (Fig. 3, 4). Chemotactic
240 motility was restored to wild-type levels by complementation *in trans* with the *cheY* gene, and even
241 exceeded that observed in the wild-type strain (Fig. 3, 4), and also the wild-type swimming
242 behaviour was restored (Fig. 5C). A wild-type strain containing an additional copy of *cheY* (WT +
243 *cheY*) displayed increased chemotactic motility compared to the wild-type strain (Fig. S3). The

244 increased chemotactic motility and migration was not due to increased growth as the *cheY* +*cheY*
245 and WT +*cheY* strains grew at the same rate as wild-type (Fig. S1).
246
247 **CheY requires the metal binding pocket but not the phosphorylation site for activity**
248 An alignment of the seed sequences for a canonical Receiver Domain (Pfam, PF00072) with
249 the *C. jejuni* CheY sequence showed that both the active site aspartic acid residue (D53) and the N-
250 terminal 'acid-pocket' aspartic acid residues (D7, D8) were well conserved (Fig. S4A). A three-
251 dimensional model of *C. jejuni* CheY, based on the *Thermotoga maritima* CheY structure [49]
252 shows that the three aspartic acid residues are predicted to cluster to form the active site (Fig. S4
253 inset). These predictions were tested experimentally using site-directed mutagenesis of aspartate
254 residues 7 and 53 to alanine (D7A and D53A) of the *cheY* gene in the *cj0046* pseudogene, to
255 eliminate either phosphorylation or metal binding, respectively, and the mutated versions were
256 introduced in the *cj0046* pseudogene in the *cheY* mutant. The *cheY*^{D53A}-complemented *cheY* mutant
257 produced flagella (Fig. 2), and showed full complementation of the *cheY* mutant with robust
258 swimming with no 'Catherine Wheel' phenotype (Fig. 5D), and restoration of chemotactic motility
259 to wild-type levels (Fig. 3, 4). In contrast, the *cheY*^{D7A} complemented *cheY* mutant was even more
260 defective in chemotactic motility (Fig. 3, 4), despite possessing polar flagella (Fig. 2). The *cheY*^{D7A}
261 strain displayed swimming in very tight repeating spirals (Fig. 5E). RT-PCR showed that all *cheY*-
262 complemented strains made a *cheY* transcript that was absent in the *cheY* mutant (Fig. S2D).
263
264 **CheA is required for chemotaxis but not for swimming motility**
265 A *cheA* mutant displayed growth comparable to the wild-type (see Fig. S1), robust swimming
266 in liquid media and flagella were observed at each pole (Fig. 2). Inactivation of *cheA* did not disrupt
267 transcription of the downstream *cheW* gene, as determined with RT-PCR (Fig. S2B). However,
268 inactivation of the *cheA* gene strongly reduced chemotactic motility to levels similar to the *cheV*

269 and *cheY* mutants (Fig. 3, 4). Introduction of the *cheA* gene *in trans* did not complement the *cheA*
270 mutant (Fig. 3, 4), but introduction of a second *cheA* copy in the wild-type strain also resulted in
271 significantly reduced chemotactic motility (Fig. S3). CheA is a large complex protein, consisting of
272 five discrete functional domains (Fig. 1). Constitutive expression of this protein likely disrupts the
273 optimal stoichiometry for effective signal transduction.
274

275 **The CheA receiver domain (CheA-Y) is dispensable for core functionality**

276 The architecture of *C. jejuni* CheA differs to that seen in *E. coli* and *B. subtilis*. (Fig. 1). CheA
277 from several members of the genus *Campylobacter* share the same architecture; the largest level of
278 sequence divergence occurs between the N-terminal Hpt domain and following HATPase_c
279 domain. The *C. jejuni* CheA protein has a C-terminal receiver domain, CheA-Y, with 58%
280 similarity (33% identity) to CheY (Fig. S4B). The multiple alignment of CheY sequences including
281 CheA-Y shows the presence of twin aspartic acid residues at the N-terminal and the active site
282 aspartate, suggesting that the acid-pocket active site is conserved (Fig. S4A). The *Campylobacter*
283 CheA architecture is by no means unique to this genus; several other species, with examples from
284 phyla spanning the bacterial section of the tree of life [50] (*Cyanobacteria*, *Proteobacteria*,
285 *Deferribacteres*, *Chloroflexi*, *Actinobacteria*, and *Firmicutes*) contain a CheA protein with the same
286 architecture (Fig. S5). To assess the role of the CheA-Y domain in the function of CheA, the *cheA*
287 gene was mutated to contain a stop-codon at position 648 ($cheA^{\Delta Rec}$), truncating the CheA protein at
288 the start of the C-terminal receiver domain. Introduction of the $cheA^{\Delta Rec}$ gene in the wild-type and
289 *cheA* mutant strain resulted in transcription of a *cheA* transcript, which was absent in the *cheA*
290 mutant (Fig. S2E). The $cheA^{\Delta Rec}$ construct complemented the *cheA* mutant better than the full length
291 *cheA* gene, with restoration of about half of chemotactic motility by the $cheA^{\Delta Rec}$ version, and no
292 complementation by the wild-type *cheA* gene (Fig. 3, 4). When introduced into the wild-type strain,
293 the $cheA^{\Delta Rec}$ strain showed higher levels of chemotactic motility than the wild-type (Fig. S3).

294 Given the similarity between CheA-Y and CheY, we also investigated the ability of the CheA-
295 Y receiver domain to complement a *cheY* mutant, by introducing the *cheA-Y* part of the *cheA* gene
296 in the *cheY* mutant (*cheY* +*cheA-Y*). Expression of the *cheA-Y* transcript was confirmed using RT-
297 PCR (Fig. S2C). The chemotactic motility phenotype of this strain was similar to the *cheY* mutant
298 (Fig. 3, 4) and the swimming behaviour showed the characteristic catherine wheels seen in the *cheY*
299 mutant (Fig. 5). Accordingly, introduction of the *cheA-Y* gene in the wild-type strain did not
300 increase chemotactic motility (Fig. S3). Thus, the sequence of the CheA-Y domain has diverged to
301 the point where it is functionally distinct from CheY in *C. jejuni*.
302

303 ***C. jejuni* encodes a putative CheX protein**

304 The *Cj0700* gene in the *C. jejuni* genome encodes an ortholog of the *H. pylori* CheZ
305 phosphatase protein [51] which functions jointly with the ChePep protein in regulating chemotaxis
306 [26] by dephosphorylation of CheY. However, a ChePep ortholog is lacking in *C. jejuni*, and there
307 is no function ascribed to Cj0700 in *C. jejuni*. A domain search of the NCTC11168 genome
308 identified the *cj0350* gene as encoding a putative CheX domain. CheX is an ancillary chemotaxis
309 protein (and least common chemotaxis-associated protein [14, 52]) known to dephosphorylate
310 CheY in *Borrelia burgdorferi* [53] and *Thermotoga maritima* [54]. The *C. jejuni* CheX sequence is
311 well conserved in the *Campylobacter* genus (but absent from the *Helicobacter* genus), although
312 divergent from the canonical CheX sequences that comprise the Pfam seed alignment PF13690. We
313 constructed a *cj0350* mutant, which showed decreased chemotactic motility, although this
314 phenotype was not rescued by complementation with *cj0350* (Fig. 6). However, complementation
315 by the gene downstream of *cj0350*, *fliN*, did restore wild-type chemotactic motility (Fig. 6),
316 suggesting that the *cheX* phenotype is probably due to a disruption of *fliN* expression. This
317 conclusion was confirmed by semi-quantitative RT-PCR, which showed that *fliN* transcript was
318 decreased in the *cheX* mutant (data not shown). To investigate the role of Cj0350, a strain

319 expressing two copies of *cj0350* was made by introduction of the *cj0350* gene *in trans* in the *cj0046*
320 pseudogene. The WT +*cj0350* strain showed bi-polar flagella (Fig. 6D) and robust swimming in
321 liquid media (see Supplementary Movie 2) but reduced chemotactic motility (Fig. 6A-C). Given
322 that CheY phosphatase activity should result in decreased chemotactic motility due to less
323 stimulation of the flagella switch, we propose that Cj0350 is a divergent CheX protein.
324

325 **Chemotaxis is required for organized biofilm formation at the air-media interface**

326 Flagella are known to be important for biofilm formation in *C. jejuni* [7-9]. We therefore
327 investigated the role of chemotaxis in biofilm formation using a glass-slide assay combined with
328 crystal violet staining and detection using a microarray scanner (employing both lasers at 532 and
329 635 nm). The wild-type strain formed a biofilm on the glass slide at the air-media interface (Fig. 7).
330 Below the air-media interface, a less-intense ~2 mm band of adhered cells was observed. All of the
331 chemotaxis mutants used in this study were defective in formation of a biofilm at the air-media
332 interface (Fig. 7). In the *cheW* mutant, the air-media interface biofilm was present, but a second
333 more intense area of adhered cells was also visible ~5 mm below the air-media interface. Both the
334 *cheV* mutant and the complemented *cheV* mutant showed defective air-media interface biofilm. The
335 *cheA* and *cheY* mutants both showed a disorganized air-media interface biofilm with a greater
336 population of submerged cells. In all cases expect for the *cheV* mutant and the $cheY^{D7A}$-
337 complemented *cheY* mutant, complementation with the respective wild-type gene restored the
338 organised interface biofilm phenotype (Fig. 7). To assess the level of shedding of cells from the
339 biofilm, the A_{600} of planktonic fraction for each assay was recorded. Inactivation of *cheY* resulted in
340 significantly fewer cells in the planktonic fraction compared to the wild-type, while the
341 complemented *cheY* mutant showed in significantly more cells in the planktonic fraction (Fig.
342 S6A). The *cheY* + $cheY^{D53A}$ complemented mutant showed a level of shedding significantly higher
343 than the *cheY* strain, again suggesting partial complementation, albeit less effective than wild-type

344 CheY. Two other *cheY* strains that showed poor chemotactic motility, the *cheY* + *cheY*^{D7A} and the
345 *cheY* + *cheV* mutants, also showed a significantly lower level of planktonic cells. Therefore, the
346 biofilm phenotype of at least the *cheY* mutant could in part be due to a disruption of normal cell
347 shedding/dispersal from the biofilm. To test the hypothesis that *C. jejuni* may require the
348 chemotaxis system to activity seek the optimal environment for growth as a biofilm, the slide
349 biofilm assay was performed using a paralysed flagella (*pflA*) mutant [46, 55]. This mutant
350 displayed low levels of biofilm formation at the air-media interface (Fig. S6B). Thus, while the
351 chemotaxis system is not required for biofilm formation *per se*, it is necessary for organized biofilm
352 formation at the air-media interface and may play a role in dispersal/shedding of cells from the
353 biofilm.
354

355 **DISCUSSION**

356 Flagellar motility plays an important role in colonisation and virulence of many bacterial
357 pathogens. While the ability to move to or from locations is an important contributor to the
358 infection process, such movement needs to be directed based on external (e.g. chemical gradient) or
359 internal stimuli (e.g. metabolic state). These stimuli can be positive or negative, with examples of
360 positive stimuli being attractants such as nutrients, while negative stimuli can be repellents such as
361 bile acids. The chemotaxis system integrates the signals from external and internal sensors through
362 a signal transduction cascade consisting of MCPs, CheW/CheV, CheA and CheY, while other
363 factors such as CheB, CheR, CheC, CheZ, or CheX may modulate and fine-tune the signal
364 transduction cascade, with diverse combinations observed throughout the bacterial kingdom [4, 56].
365 In this study we have dissected the core chemotaxis signalling pathway of the important
366 foodborne zoonotic pathogen *C. jejuni*, which is the most common bacterial cause of gastroenteritis
367 in the developed world. Directed motility is central to the process of intestinal colonisation by *C.*
368 *jejuni*, as mutants defective in motility or chemotaxis are either unable to colonise or show

369 significantly reduced efficiency of colonisation [38, 42]. Although *C. jejuni* shares many
370 components of the core chemotaxis pathway with model organisms such as *E. coli* and *B. subtilis*,
371 its chemotaxis system contains several additional components and modifications, and in this study
372 we have systematically characterised these core chemotaxis pathway using a combination of
373 phenotypic assays and gene inactivation and complementation experiments.
374

375 ***C. jejuni* CheW and CheV adaptor proteins have distinct roles**

376 *Campylobacter* is not exceptional in containing both CheV and CheW proteins. Although
377 CheW is the most common chemotaxis 'adaptor' protein (found in nearly 100% of genomes
378 containing the core chemotaxis components [14], CheV was found in almost 40% of chemotaxis-
379 positive genomes [14] and three genomes (*B. thuringiensis*, *B. weihenstephanensis*, and *L.*
380 *monocytogenes*) were found to contain only CheV, and no CheW suggesting that CheV alone can
381 function in the MCP-CheA complex [14]. In this study, the chemotaxis phenotype of the *cheW*
382 mutant is the least severe, suggesting that CheV does function to elicit some signal transduction.
383 Similar results were obtained in *B. subtilis* [57] and further showed that the CheW domain of CheV
384 was sufficient for signal transduction. A direct protein-protein interaction between CheV and Tlp4
385 (deoxycholate sensor, Cj0262c), Tlp6 (TCA intermediates sensor, Cj0448c), and Tlp8 (redox sensor
386 CetZ) has been documented [58] and Hartley-Tassell *et al* further used Yeast Two- and Three-
387 Hybrid analysis and immunoprecipitation to show that Tlp1 interacts with both CheW and CheV,
388 although the interaction with CheV was much stronger and localised to the CheV-W domain [41].
389 Their work also showed that both *cheV* and *cheW* mutants had chemotactic motility defects in
390 Brucella media although chemotaxis towards aspartate was still competent in either mutant.
391 Similarly, the Cj0371 protein was shown to interact with the CheV protein, and influence ATPase
392 activity of CheA [59], suggesting that multiple systems engage in the chemotaxis pathway to
393 modulate signal transduction. An evolutionary genomics study showed that the presence of CheV

394 correlated with increased numbers of MCPs and proposed that CheV functions to accommodate
395 signal transduction from a specific group of MCPs, exemplified by the *Salmonella* McpC chemo-
396 receptor [24]. None of the ten *C. jejuni* MCPs share the architecture of the McpC-type sensor.
397 Moreover, *H. pylori* genomes encode only four chemotaxis sensors and three CheV proteins, all of
398 which accept phosphate from CheA [60]. The C-terminal receiver domain on CheV most likely
399 refines the function of this protein. It has previously been proposed that CheV acts as a phosphate
400 sink, normalizing over-stimulation of CheA [24, 61, 62]. The observation that expressing two
401 copies of CheV in *C. jejuni* reduces chemotactic motility (Fig. 3, 4) supports this theory, as
402 increasing the level of the CheV protein will divert phosphate flow from CheY to CheV. The fact
403 that the chemotaxis phenotype of the WT +*cheV* strain is more severe compared to the WT +*cheX*
404 strain suggests that the phosphate sink is more effective at dampening signal transduction than
405 CheX-mediated dephosphorylation of CheY. Organisms lacking CheY-phosphatases may also
406 utilize a phosphate sink mechanism to modulate chemotaxis.
407

408 **Role of CheY domains**

409 The CheY protein is the final effector protein in the signal transduction cascade, directly
410 interacting with the flagellar switch to alter rotation between clockwise and counter-clockwise
411 rotation. Our observation that the *cheY*^{D53A} variant could restore both chemotactic motility and
412 darting swimming in the *cheY* mutant (Fig. 3, 4) suggests that either a) unphosphorylated CheY can
413 interact with the flagella switch or b) the conserved aspartate 53 residue is not the only site of
414 activating phosphorylation. Sequence alignment of *C. jejuni* CheY with the seed receiver domain
415 alignment unambiguously identifies the putative site of phosphorylation and a structural model
416 clearly places Aspartate 53 in the acid pocket active site. Expression of CheY^{D53A} from the *fdxA*
417 promoter may result in expression of the protein at increased levels. Indeed, expression of wild-type
418 CheY from the *fdxA* promoter significantly stimulated chemotactic motility (Fig. 3, 4). Based on the

419 CheY^{D53A} data, the chemotactic motility observed in the complemented *cheY* mutant may be a
420 mixture of CheY and CheY-P interaction at the flagella switch. If unphosphorylated CheY can
421 modify the flagella switch operation, the question of resetting the chemotaxis system in *C. jejuni*
422 becomes all the more intriguing. If one further considers the C-terminal receiver domain of CheA as
423 a further phosphate sink, the complete model of phosphate-flow in *C. jejuni* chemotaxis becomes a
424 complex story. The CheA-Y domain has all the hallmarks of the classical receiver domain and
425 appears to be dispensable for the core signal transduction function. Moreover, CheA-Y is no
426 substitute for CheY as the *cheA-Y* gene could not complement the inactivation of *cheY* (Fig. 3, 4).
427 Residues that are known to be important for binding the flagella switch (T87, Y106, and K109 (*E.*
428 *coli* numbering [63])) are conserved in CheA-Y and amino acid differences between CheY and
429 CheA-Y are spread across the entire sequence, and not localized to the β4-α4 region, which shows
430 the largest structural changes following phosphorylation [64, 65]. Sequence divergence resulting in
431 loss of chemotactic function is well documented: *R. sphaeroides che* genes only partially restore
432 taxis in *E. coli* [66]. Thus, the *C. jejuni* CheY/CheA-Y proteins provide a good model for studying
433 mutational drift resulting in loss or change of function. *C. jejuni* CheA lacks the P2 domain found in
434 *E. coli* and *B. subtilis* CheA (Fig. 1), which raises the question of how it interacts with CheY.
435 Certainly, Parrish *et al* detected interactions between CheA and CheY [58]. The C-terminal CheA-
436 Y domain would be a good candidate since similar folds may allow homo-dimer formation.
437 However, since CheA$^{\Delta Rec}$ restores signalling, the CheA-Y domain is not the likely interaction
438 partner for CheY.
439

440 **Cj0350, a novel variant of CheX?**

441 In this study we have identified a potential CheX ortholog, represented by the Cj0350 protein.
442 Although inactivation of the *cj0350* gene did affect chemotaxis, this was probably due to a polar
443 effect on the downstream *fliN* gene, and hence we cannot be certain about the role of Cj0350 in

444 chemotaxis yet. The Cj0350 protein may be a novel variant of CheX, representing a
445 *Campylobacter*-specific chemotaxis adaptation in the Epsilonproteobacteria, as no CheX ortholog
446 could be detected in any available *Helicobacter* genome. The primary sequence of the putative
447 CheX protein identified in this study is divergent from the canonical CheX sequence. Thus, in
448 organisms where no current phosphatase has been identified, cryptic phosphatase proteins may yet
449 be discovered. In addition to CheX and CheZ, a number of other CheY phosphatases have been
450 characterized. *B. subtilis* uses CheC, CheD, and a FliY/N fusion protein [52, 67, 68]. However,
451 chemotaxis systems lacking any clear phosphatases are also known (~20% of chemotaxis positive
452 genomes [14]); for instance, *Rhodobacter sphaeroides*, *Rhodospirillum centenum*, and
453 *Sinorhizobium meliloti* have complex chemotaxis systems but lack known CheY-phosphatases [25,
454 66]. *H. pylori* further regulates CheZ activity by complex formation with the novel chemotaxis
455 protein ChePep [26, 69]. *Campylobacter jejuni* contains a ChePep homolog (NCTC11168 -
456 Cj1178c), which can complement an *H. pylori chepep* mutant [69] although the role of this protein
457 in chemotaxis in *C. jejuni* is currently not known.
458

459 **Chemotaxis and Biofilm formation**

460 Previous studies have implicated chemotaxis sensors in biofilm formation. Tlp3 (Cj1564)
461 mutants showed increased biofilm formation [30], while CetZ (Tlp8) mutants showed decreased
462 biofilm formation [28]. We show that removing each component of the chemotaxis pathway results
463 in disorganised biofilm formation and this phenotype can be rescued by complementation. Thus, the
464 chemotaxis system likely has a role in coordinating biofilm formation, and this coordinating role
465 may extend to shedding and dispersal of cells from the biofilm. This study is therefore the first to
466 present a role for signal transduction in the active dispersal of cells from a *C. jejuni* biofilm. In
467 processing environments, biofilms present a reservoir of cells that can subsequently re-contaminate
468 the food chain highlighting the need to learn more about biofilm dispersal.

469

470 **A model for the *C. jejuni* core chemotaxis system**

471 Based on the data presented, we propose a model for chemotaxis in *C. jejuni* that has more
472 similarity to the Gram positive model of chemotaxis, as exemplified by *B. subtilis* (Fig. 9). Based
473 on the *E. coli* paradigm, deleting any one of the core chemotaxis proteins should result in counter-
474 clockwise flagella rotation and darting motility (as phospho-CheY results in clockwise flagella
475 rotation and tumbling). Our data show that *cheW-V-A-Y* mutants have impaired chemotactic
476 motility suggestive of a tumbling swimming phenotype (clockwise flagella rotation). Indeed, the
477 *cheY* mutant cells are observed to swim in clockwise 'catherine wheel' loops, while the
478 complemented *cheY +cheY* strain swims as the wild-type. In the *B. subtilis* model, a *cheY* null
479 mutant results in tumbling motility [70], so reducing CheY phosphorylation (*cheA* and/or *cheW*
480 mutants) will result in clockwise flagella rotation and tumbling swimming. Thus, in this respect, the
481 *B. subtilis* model is more appropriate than the *E. coli* model for *C. jejuni*. A phylogenomic
482 classification of bacterial chemotaxis systems placed all the known *Campylobacter* genomes into a
483 particular group 'F3' [14], a group that also represents chemotaxis systems from other members of
484 the Epsilon proteobacteria. Based on the finding of a putative CheX protein, this proposed *C. jejuni*
485 chemotaxis system does not fit into any of the existing models suggested by Wuichet and Zhulin
486 [14]. However, as new genome sequences emerge and are characterised, it is likely that existing
487 classifications will need updating. The model presented in Figure 8 includes the *H. pylori* CheZ
488 homolog, Cj0700. It is known that the *H. pylori* CheZ homolog (HP0170, [71]) has phosphatase
489 activity on CheY, CheA, and CheV2 [51], however, as yet no evidence of the involvement of
490 Cj0700 in chemotaxis has been reported. It is possible that *C. jejuni* may use both CheZ and CheX
491 to dephosphorylate CheY.

492

493 **Conclusions**

494 The ability to couple flagella rotation with environmental sensing is an effective adaptive
495 mechanism allowing bacteria to seek an optimum environment. While chemotaxis systems from
496 model organisms provide an effective model for studying signal transduction in non-paradigm
497 organisms, species-specific modulations and augmentations abound and require focussed
498 investigation. Our results from the analysis of the core chemotaxis system of *C. jejuni* suggests that
499 a unique chemotaxis system has evolved in *Campylobacter*, which has more commonality with
500 Gram-positive organisms. Such a model may inform on chemotaxis in other Epsilon proteobacteria,
501 such as the human pathogens *Campylobacter coli* and *Arcobacter butzleri*, and other organisms that
502 share elements of the *Campylobacter* chemotaxis system and provides a further paradigm for
503 chemotaxis signal transduction.
504

505 **Acknowledgments**
506 The authors wish to thank Dr Henri Tapp for assistance with statistical evaluations, and members of
507 the former IFR *Campylobacter* research group for helpful discussions. We would also like to thank
508 Rachael Stanley for electron microscopy and Maddy Houchen and Robert Hindmarsh for
509 microbiology media support.
510

511 **Funding statement**
512 The authors gratefully acknowledge the support of the Biotechnology and Biological Sciences
513 Research Council (BBSRC) via the Gut Health and Food Safety Institute Strategic Programme
514 (BB/J004529/1). The funders had no role in study design, data collection and analysis, decision to
515 publish, or preparation of the manuscript. The authors have declared that no competing interests
516 exist.
517
518

519 **REFERENCES**

520 1. Nichols GL, Richardson JF, Sheppard SK, Lane C, Sarran C. Campylobacter epidemiology:
521 a descriptive study reviewing 1 million cases in England and Wales between 1989 and 2011.
522 BMJ Open. 2012;2(4):e001179. doi: 10.1136/bmjopen-2012-001179. PubMed PMID:
523 22798256.
524 2. Tam CC, Higgins CD, Neal KR, Rodrigues LC, Millership SE, O'Brien SJ, et al. Chicken
525 Consumption and Use of Acid-Suppressing Medications as Risk Factors for Campylobacter
526 Enteritis, England. Emerging Infectious Diseases. 2009;15(9):1402-8. doi:
527 10.3201/eid1509.080773. PubMed PMID: PMC2819848.
528 3. Poropatich KO, Walker CL, Black RE. Quantifying the association between Campylobacter
529 infection and Guillain-Barre syndrome: a systematic review. J Health Popul Nutr.
530 2010;28(6):545-52. PubMed PMID: 21261199.
531 4. Lertsethtakarn P, Ottemann KM, Hendrixson DR. Motility and chemotaxis in Campylobacter
532 and Helicobacter. Annu Rev Microbiol. 2011;65:389-410. doi: 10.1146/annurev-micro-
533 090110-102908. PubMed PMID: 21939377.
534 5. Gao B, Lara-Tejero M, Lefebre M, Goodman AL, Galan JE. Novel components of the
535 flagellar system in epsilonproteobacteria. MBio. 2014;5(3):e01349-14. doi:
536 10.1128/mBio.01349-14. PubMed PMID: 24961693.
537 6. Asakura H, Hashii N, Uema M, Kawasaki N, Sugita-Konishi Y, Igimi S, et al. Campylobacter
538 jejuni pdxA affects flagellum-mediated motility to alter host colonization. PloS one.
539 2013;8(8):e70418. doi: 10.1371/journal.pone.0070418. PubMed PMID: 23936426.
540 7. Reuter M, Mallett A, Pearson BM, van Vliet AH. Biofilm formation by *Campylobacter jejuni*
541 is increased under aerobic conditions. Appl Environ Microbiol. 2010;76(7):2122-8. doi:
542 10.1128/AEM.01878-09. PubMed PMID: 20139307.
543 8. Svensson SL, Pryjma M, Gaynor EC. Flagella-mediated adhesion and extracellular DNA
544 release contribute to biofilm formation and stress tolerance of Campylobacter jejuni. PLoS
545 One. 2014;9(8):e106063. doi: 10.1371/journal.pone.0106063. PubMed PMID: 25166748.
546 9. Brown HL, Reuter M, Salt LJ, Cross KL, Betts RP, van Vliet AH. Chicken juice enhances
547 surface attachment and biofilm formation of Campylobacter jejuni. Appl Environ Microbiol.
548 2014;80(22):7053-60. doi: 10.1128/AEM.02614-14. PubMed PMID: 25192991.
549 10. Baldvinsson SB, Sorensen MC, Vegge CS, Clokie MR, Brondsted L. Campylobacter jejuni
550 motility is required for infection of the flagellotropic bacteriophage F341. Appl Environ
551 Microbiol. 2014;80(22):7096-106. doi: 10.1128/AEM.02057-14. PubMed PMID: 25261508.
552 11. Wadhams GH, Armitage JP. Making sense of it all: bacterial chemotaxis. Nat Rev Mol Cell
553 Biol. 2004;5(12):1024-37. doi: 10.1038/nrm1524. PubMed PMID: 15573139.
554 12. Baker MD, Wolanin PM, Stock JB. Signal transduction in bacterial chemotaxis. Bioessays.
555 2006;28(1):9-22. doi: 10.1002/bies.20343. PubMed PMID: 16369945.
556 13. Hazelbauer GL, Lai WC. Bacterial chemoreceptors: providing enhanced features to two-
557 component signaling. Curr Opin Microbiol. 2010;13(2):124-32. doi:
558 10.1016/j.mib.2009.12.014. PubMed PMID: 20122866.
559 14. Wuichet K, Zhulin IB. Origins and Diversification of a Complex Signal Transduction System
560 in Prokaryotes. Science Signaling. 2010;3(128):ra50-ra. doi: 10.1126/scisignal.2000724.
561 15. Patteson AE, Gopinath A, Goulian M, Arratia PE. Running and tumbling with E. coli in
562 polymeric solutions. Sci Rep. 2015;5:15761. doi: 10.1038/srep15761. PubMed PMID:
563 26507950.
564 16. Krell T, Lacal J, Munoz-Martinez F, Reyes-Darias JA, Cadirci BH, Garcia-Fontana C, et al.
565 Diversity at its best: bacterial taxis. Environ Microbiol. 2011;13(5):1115-24. doi:
566 10.1111/j.1462-2920.2010.02383.x. PubMed PMID: 21087385.

567 17. Alon U, Camarena L, Surette MG, Aguera y Arcas B, Liu Y, Leibler S, et al. Response
568 regulator output in bacterial chemotaxis. Embo J. 1998;17(15):4238-48. doi:
569 10.1093/emboj/17.15.4238. PubMed PMID: 9687492.
570 18. Cluzel P, Surette M, Leibler S. An ultrasensitive bacterial motor revealed by monitoring
571 signaling proteins in single cells. Science. 2000;287(5458):1652-5. PubMed PMID:
572 10698740.
573 19. Fuhrer DK, Ordal GW. Bacillus subtilis CheN, a homolog of CheA, the central regulator of
574 chemotaxis in Escherichia coli. J Bacteriol. 1991;173(23):7443-8. PubMed PMID: 1938941.
575 20. Garrity LF, Ordal GW. Chemotaxis in *Bacillus subtilis*: how bacteria monitor environmental
576 signals. Pharmacol Ther. 1995;68(1):87-104. PubMed PMID: 8604438.
577 21. Martin AC, Wadhams GH, Armitage JP. The roles of the multiple CheW and CheA
578 homologues in chemotaxis and in chemoreceptor localization in *Rhodobacter sphaeroides*.
579 Mol Microbiol. 2001;40(6):1261-72. PubMed PMID: 11442826.
580 22. Boukhvalova MS, Dahlquist FW, Stewart RC. CheW binding interactions with CheA and Tar.
581 Importance for chemotaxis signaling in *Escherichia coli*. J Biol Chem. 2002;277(25):22251-
582 9. doi: 10.1074/jbc.M110908200. PubMed PMID: 11923283.
583 23. Parkinson JS, Hazelbauer GL, Falke JJ. Signaling and sensory adaptation in *Escherichia coli*
584 chemoreceptors: 2015 update. Trends in Microbiology. 2015;23(5):257-66. doi:
585 http://dx.doi.org/10.1016/j.tim.2015.03.003.
586 24. Ortega DR, Zhulin IB. Evolutionary Genomics Suggests That CheV Is an Additional Adaptor
587 for Accommodating Specific Chemoreceptors within the Chemotaxis Signaling Complex.
588 PLoS computational biology. 2016;12(2):e1004723. doi: 10.1371/journal.pcbi.1004723.
589 PubMed PMID: 26844549.
590 25. Porter SL, Wadhams GH, Armitage JP. Signal processing in complex chemotaxis pathways.
591 Nat Rev Microbiol. 2011;9(3):153-65. doi: 10.1038/nrmicro2505. PubMed PMID: 21283116.
592 26. Lertsethtakarn P, Howitt MR, Castellon J, Amieva MR, Ottemann KM. *Helicobacter pylori*
593 CheZ(HP) and ChePep form a novel chemotaxis-regulatory complex distinct from the core
594 chemotaxis signaling proteins and the flagellar motor. Mol Microbiol. 2015;97(6):1063-78.
595 doi: 10.1111/mmi.13086. PubMed PMID: 26061894.
596 27. Day CJ, King RM, Shewell LK, Tram G, Najnin T, Hartley-Tassell LE, et al. A direct-sensing
597 galactose chemoreceptor recently evolved in invasive strains of Campylobacter jejuni. Nat
598 Commun. 2016;7:13206. doi: 10.1038/ncomms13206. PubMed PMID: 27762269.
599 28. Chandrashekhar K, Gangaiah D, Pina-Mimbela R, Kassem, II, Jeon BH, Rajashekara G.
600 Transducer like proteins of *Campylobacter jejuni* 81-176: role in chemotaxis and colonization
601 of the chicken gastrointestinal tract. Front Cell Infect Microbiol. 2015;5:46. doi:
602 10.3389/fcimb.2015.00046. PubMed PMID: 26075188.
603 29. Li Z, Lou H, Ojcius DM, Sun A, Sun D, Zhao J, et al. Methyl-accepting chemotaxis proteins
604 3 and 4 are responsible for *Campylobacter jejuni* chemotaxis and jejuna colonization in mice
605 in response to sodium deoxycholate. J Med Microbiol. 2014;63(Pt 3):343-54. doi:
606 10.1099/jmm.0.068023-0. PubMed PMID: 24403598.
607 30. Rahman H, King RM, Shewell LK, Semchenko EA, Hartley-Tassell LE, Wilson JC, et al.
608 Characterisation of a multi-ligand binding chemoreceptor CcmL (Tlp3) of *Campylobacter*
609 *jejuni*. PLoS Pathog. 2014;10(1):e1003822. doi: 10.1371/journal.ppat.1003822. PubMed
610 PMID: 24391495.
611 31. Vegge CS, Brondsted L, Li YP, Bang DD, Ingmer H. Energy taxis drives *Campylobacter*
612 *jejuni* toward the most favorable conditions for growth. Appl Environ Microbiol.
613 2009;75(16):5308-14. doi: 10.1128/aem.00287-09. PubMed PMID: 19542337.
614 32. Hendrixson DR, Akerley BJ, DiRita VJ. Transposon mutagenesis of *Campylobacter jejuni*
615 identifies a bipartite energy taxis system required for motility. Mol Microbiol.
616 2001;40(1):214-24. PubMed PMID: 11298288.

617 33. Reuter M, van Vliet AH. Signal balancing by the CetABC and CetZ chemoreceptors controls
618 energy taxis in *Campylobacter jejuni*. PLoS One. 2013;8(1):e54390. doi:
619 10.1371/journal.pone.0054390. PubMed PMID: 23382896.
620 34. Dwivedi R, Nothaft H, Garber J, Xin Kin L, Stahl M, Flint A, et al. L-fucose influences
621 chemotaxis and biofilm formation in *Campylobacter jejuni*. Mol Microbiol. 2016. doi:
622 10.1111/mmi.13409. PubMed PMID: 27145048.
623 35. Lubke AL, Minatelli S, Riedel T, Lugert R, Schober I, Sproer C, et al. The transducer-like
624 protein Tlp12 of Campylobacter jejuni is involved in glutamate and pyruvate chemotaxis.
625 BMC Microbiol. 2018;18(1):111. doi: 10.1186/s12866-018-1254-0. PubMed PMID:
626 30200886.
627 36. Chandrashekhar K, Kassem, II, Rajashekara G. Campylobacter jejuni transducer like proteins:
628 Chemotaxis and beyond. Gut Microbes. 2017;8(4):323-34. doi:
629 10.1080/19490976.2017.1279380. PubMed PMID: 28080213.
630 37. Takata T, Fujimoto S, Amako K. Isolation of nonchemotactic mutants of *Campylobacter*
631 *jejuni* and their colonization of the mouse intestinal tract. Infect Immun. 1992;60(9):3596-
632 600. PubMed PMID: 1500167.
633 38. Yao R, Burr DH, Guerry P. CheY-mediated modulation of *Campylobacter jejuni* virulence.
634 Mol Microbiol. 1997;23(5):1021-31. PubMed PMID: 9076738.
635 39. Hendrixson DR, DiRita VJ. Identification of *Campylobacter jejuni* genes involved in
636 commensal colonization of the chick gastrointestinal tract. Mol Microbiol. 2004;52(2):471-
637 84. doi: 10.1111/j.1365-2958.2004.03988.x. PubMed PMID: 15066034.
638 40. Bereswill S, Fischer A, Plickert R, Haag LM, Otto B, Kuhl AA, et al. Novel murine infection
639 models provide deep insights into the "menage a trois" of *Campylobacter jejuni*, microbiota
640 and host innate immunity. PLoS One. 2011;6(6):e20953. doi: 10.1371/journal.pone.0020953.
641 PubMed PMID: 21698299.
642 41. Hartley-Tassell LE, Shewell LK, Day CJ, Wilson JC, Sandhu R, Ketley JM, et al.
643 Identification and characterization of the aspartate chemosensory receptor of *Campylobacter*
644 *jejuni*. Mol Microbiol. 2010;75(3):710-30. doi: 10.1111/j.1365-2958.2009.07010.x. PubMed
645 PMID: 20025667.
646 42. de Vries SP, Linn A, Macleod K, MacCallum A, Hardy SP, Douce G, et al. Analysis of
647 Campylobacter jejuni infection in the gnotobiotic piglet and genome-wide identification of
648 bacterial factors required for infection. Sci Rep. 2017;7:44283. doi: 10.1038/srep44283.
649 PubMed PMID: 28281647.
650 43. Gao B, Vorwerk H, Huber C, Lara-Tejero M, Mohr J, Goodman AL, et al. Metabolic and
651 fitness determinants for in vitro growth and intestinal colonization of the bacterial pathogen
652 Campylobacter jejuni. PLoS Biol. 2017;15(5):e2001390. doi: 10.1371/journal.pbio.2001390.
653 PubMed PMID: 28542173.
654 44. Porcelli I, Reuter M, Pearson BM, Wilhelm T, van Vliet AH. Parallel evolution of genome
655 structure and transcriptional landscape in the Epsilonproteobacteria. BMC Genomics.
656 2013;14:616. doi: 10.1186/1471-2164-14-616. PubMed PMID: 24028687.
657 45. Heimbrook ME, Wang WL, Campbell G. Staining bacterial flagella easily. J Clin Microbiol.
658 1989;27(11):2612-5. PubMed PMID: 2478573.
659 46. Reuter M, Periago PM, Mulholland F, Brown HL, van Vliet AH. A PAS domain-containing
660 regulator controls flagella-flagella interactions in Campylobacter jejuni. Front Microbiol.
661 2015;6:770. doi: 10.3389/fmicb.2015.00770. PubMed PMID: 26284050.
662 47. Alexander RP, Lowenthal AC, Harshey RM, Ottemann KM. CheV: CheW-like coupling
663 proteins at the core of the chemotaxis signaling network. Trends Microbiol. 2010;18(11):494-
664 503. doi: 10.1016/j.tim.2010.07.004. PubMed PMID: 20832320.

665 48. Lauga E, DiLuzio WR, Whitesides GM, Stone HA. Swimming in circles: motion of bacteria
666 near solid boundaries. Biophys J. 2006;90(2):400-12. doi: 10.1529/biophysj.105.069401.
667 PubMed PMID: 16239332.
668 49. Usher KC, de la Cruz AF, Dahlquist FW, Swanson RV, Simon MI, Remington SJ. Crystal
669 structures of CheY from Thermotoga maritima do not support conventional explanations for
670 the structural basis of enhanced thermostability. Protein Sci. 1998;7(2):403-12. doi:
671 10.1002/pro.5560070221. PubMed PMID: 9521117.
672 50. Hug LA, Baker BJ, Anantharaman K, Brown CT, Probst AJ, Castelle CJ, et al. A new view
673 of the tree of life. Nature Microbiology. 2016:16048. doi: 10.1038/nmicrobiol.2016.48.
674 51. Lertsethtakarn P, Ottemann KM. A remote CheZ orthologue retains phosphatase function.
675 Mol Microbiol. 2010;77(1):225-35. doi: 10.1111/j.1365-2958.2010.07200.x. PubMed PMID:
676 20497335.
677 52. Silversmith RE. Auxiliary phosphatases in two-component signal transduction. Curr Opin
678 Microbiol. 2010;13(2):177-83. doi: 10.1016/j.mib.2010.01.004. PubMed PMID: 20133180.
679 53. Motaleb MA, Miller MR, Li C, Bakker RG, Goldstein SF, Silversmith RE, et al. CheX is a
680 phosphorylated CheY phosphatase essential for *Borrelia burgdorferi* chemotaxis. J Bacteriol.
681 2005;187(23):7963-9. doi: 10.1128/jb.187.23.7963-7969.2005. PubMed PMID: 16291669.
682 54. Park SY, Chao X, Gonzalez-Bonet G, Beel BD, Bilwes AM, Crane BR. Structure and function
683 of an unusual family of protein phosphatases: the bacterial chemotaxis proteins CheC and
684 CheX. Mol Cell. 2004;16(4):563-74. doi: 10.1016/j.molcel.2004.10.018. PubMed PMID:
685 15546616.
686 55. Yao R, Burr DH, Doig P, Trust TJ, Niu H, Guerry P. Isolation of motile and non-motile
687 insertional mutants of *Campylobacter jejuni*: the role of motility in adherence and invasion of
688 eukaryotic cells. Mol Microbiol. 1994;14(5):883-93. PubMed PMID: 7715450.
689 56. Micali G, Endres RG. Bacterial chemotaxis: information processing, thermodynamics, and
690 behavior. Curr Opin Microbiol. 2016;30:8-15. doi: 10.1016/j.mib.2015.12.001. PubMed
691 PMID: 26731482.
692 57. Rosario MM, Fredrick KL, Ordal GW, Helmann JD. Chemotaxis in Bacillus subtilis requires
693 either of two functionally redundant CheW homologs. J Bacteriol. 1994;176(9):2736-9.
694 PubMed PMID: 8169224.
695 58. Parrish JR, Yu J, Liu G, Hines JA, Chan JE, Mangiola BA, et al. A proteome-wide protein
696 interaction map for *Campylobacter jejuni*. Genome Biol. 2007;8(7):R130. doi: 10.1186/gb-
697 2007-8-7-r130. PubMed PMID: 17615063.
698 59. Du X, Wang N, Ren F, Tang H, Jiao X, Huang J. cj0371: A Novel Virulence-Associated Gene
699 of Campylobacter jejuni. Front Microbiol. 2016;7:1094. doi: 10.3389/fmicb.2016.01094.
700 PubMed PMID: 27471500.
701 60. Jimenez-Pearson MA, Delany I, Scarlato V, Beier D. Phosphate flow in the chemotactic
702 response system of *Helicobacter pylori*. Microbiology (Reading, England). 2005;151(Pt
703 10):3299-311. doi: 10.1099/mic.0.28217-0. PubMed PMID: 16207913.
704 61. Karatan E, Saulmon MM, Bunn MW, Ordal GW. Phosphorylation of the response regulator
705 CheV is required for adaptation to attractants during *Bacillus subtilis* chemotaxis. J Biol
706 Chem. 2001;276(47):43618-26. doi: 10.1074/jbc.M104955200. PubMed PMID: 11553614.
707 62. Pittman MS, Goodwin M, Kelly DJ. Chemotaxis in the human gastric pathogen *Helicobacter*
708 *pylori*: different roles for CheW and the three CheV paralogues, and evidence for CheV2
709 phosphorylation. Microbiology (Reading, England). 2001;147(Pt 9):2493-504. doi:
710 10.1099/00221287-147-9-2493. PubMed PMID: 11535789.
711 63. Schuster M, Silversmith RE, Bourret RB. Conformational coupling in the chemotaxis
712 response regulator CheY. Proc Natl Acad Sci U S A. 2001;98(11):6003-8. doi:
713 10.1073/pnas.101571298. PubMed PMID: 11353835.

714 64. Sola M, Lopez-Hernandez E, Cronet P, Lacroix E, Serrano L, Coll M, et al. Towards
715 understanding a molecular switch mechanism: thermodynamic and crystallographic studies
716 of the signal transduction protein CheY. J Mol Biol. 2000;303(2):213-25. doi:
717 10.1006/jmbi.2000.4507. PubMed PMID: 11023787.
718 65. Lee SY, Cho HS, Pelton JG, Yan D, Berry EA, Wemmer DE. Crystal structure of activated
719 CheY. Comparison with other activated receiver domains. J Biol Chem. 2001;276(19):16425-
720 31. doi: 10.1074/jbc.M101002200. PubMed PMID: 11279165.
721 66. Porter SL, Wadhams GH, Armitage JP. *Rhodobacter sphaeroides*: complexity in chemotactic
722 signalling. Trends Microbiol. 2008;16(6):251-60. doi: 10.1016/j.tim.2008.02.006. PubMed
723 PMID: 18440816.
724 67. Szurmant H, Bunn MW, Cannistraro VJ, Ordal GW. Bacillus subtilis hydrolyzes CheY-P at
725 the location of its action, the flagellar switch. J Biol Chem. 2003;278(49):48611-6. doi:
726 10.1074/jbc.M306180200. PubMed PMID: 12920116.
727 68. Szurmant H, Muff TJ, Ordal GW. Bacillus subtilis CheC and FliY are members of a novel
728 class of CheY-P-hydrolyzing proteins in the chemotactic signal transduction cascade. J Biol
729 Chem. 2004;279(21):21787-92. doi: 10.1074/jbc.M311497200. PubMed PMID: 14749334.
730 69. Howitt MR, Lee JY, Lertsethtakarn P, Vogelmann R, Joubert LM, Ottemann KM, et al.
731 ChePep controls *Helicobacter pylori* Infection of the gastric glands and chemotaxis in the
732 Epsilonproteobacteria. MBio. 2011;2(4). doi: 10.1128/mBio.00098-11. PubMed PMID:
733 21791582.
734 70. Bischoff DS, Ordal GW. *Bacillus subtilis* chemotaxis: a deviation from the *Escherichia coli*
735 paradigm. Mol Microbiol. 1992;6(1):23-8. PubMed PMID: 1738311.
736 71. Terry K, Go AC, Ottemann KM. Proteomic mapping of a suppressor of non-chemotactic
737 cheW mutants reveals that Helicobacter pylori contains a new chemotaxis protein. Mol
738 Microbiol. 2006;61(4):871-82. doi: 10.1111/j.1365-2958.2006.05283.x. PubMed PMID:
739 16879644.
740 72. Parkhill J, Wren BW, Mungall K, Ketley JM, Churcher C, Basham D, et al. The genome
741 sequence of the food-borne pathogen *Campylobacter jejuni* reveals hypervariable sequences.
742 Nature. 2000;403(6770):665-8. doi: 10.1038/35001088. PubMed PMID: 10688204.
743

745 **Table 1** | Bacterial strains used in this study.

Strain	Description [a]
***E. coli* strain**	
Top10	General cloning strain
***C. jejuni* strains**	
NCTC 11168	Wild-type *C. jejuni* [72]
11168 Δ*cheY*	NCTC 11168 *cj1118c::kan*^{R}
11168 Δ*cheW*	NCTC 11168 *cj0283c::kan*^{R}
11168 Δ*cheA*	NCTC 11168 *cj0284c::cat*^{R}
11168 Δ*cheV*	NCTC 11168 *cj0285c::kan*^{R}
11168 Δ*cheY* +*cheY*^{fdxApr*}	NCTC 11168 *cj1118c::kan*^{R} *cj0046*::*cj1118c*^{fdxApr}**cat*^{R}
11168 Δ*cheY* +*cheYD53A*^{fdxApr*}	NCTC 11168 *cj1118c::kan*^{R} *cj0046*::*cj1118c*^{D53AfdxApr}**cat*^{R}
11168 Δ*cheY* +*cheYD7A*^{fdxApr*}	NCTC 11168 *cj1118c::kan*^{R} *cj0046*::*cj1118c*^{D7AfdxApr}**cat*^{R}
11168 Δ*cheY* +*cheA-Y*^{fdxApr*}	NCTC 11168 *cj1118c::kan*^{R} *cj0046*::*cj0284c*$^{648\text{-}769_fdxApr}$**cat*^{R}
11168 Δ*cheW* +*cheW*^{fdxApr*}	NCTC 11168 *cj0283c::kan*^{R} *cj0046*::*cj0283c*^{fdxApr}**cat*^{R}
11168 Δ*cheA* +*cheA*^{fdxApr*}	NCTC 11168 *cj0284c::cat*^{R} *cj0046*::*cj0284c*^{fdxApr}**kan*^{R}
11168 Δ*cheA* +*cheARec*^{fdxApr*}	NCTC 11168 *cj0284c::cat*^{R} *cj0046*::*cj0284c*ΔRec^{fdxApr}**kan*^{R}
11168 Δ*cheV* +*cheV*^{fdxApr*}	NCTC 11168 *cj0285c::kan*^{R} *cj0046*::*cj0285c*^{fdxApr}**cat*^{R}
11168 Δ*cheW* +*cheV*^{fdxApr*}	NCTC 11168 *cj0283c::kan*^{R} *cj0046*::*cj0285c*^{fdxApr}**cat*^{R}
11168 *cheY*^{fdxApr*}	NCTC 11168 *cj0046*::*cj1118c*^{fdxApr}**cat*^{R}
11168 *cheYD53A*^{fdxApr*}	NCTC 11168 *cj0046*::*cj1118c*^{D53AfdxApr}**cat*^{R}
11168 *cheW*^{fdxApr*}	NCTC 11168 *cj0046*::*cj0283c*^{fdxApr}**cat*^{R}
11168 *cheA*^{fdxApr*}	NCTC 11168 *cj0046*::*cj0284c*^{fdxApr}**kan*^{R}
11168 *cheX*^{fdxApr*}	NCTC 11168 *cj0046*::*cj0350c*^{fdxApr}**kan*^{R}
11168 Δ*pflA*	NCTC11168 *cj1565c::kan*^{R}

746 a. *kan*^{R}, kanamycin resistance cassette; *cat*^{R}, chloramphenicol resistance cassette; * denotes
747 complementation construct: ^{fdxApr}, gene under control of the constitutive *fdxA* promoter.
748

749 **Table 2** | Plasmids used in this study.

Plasmids	**Description** [a]
pNEB193	General cloning vector (NEB)
pCfdxA	Complementation plasmid containing *cj0046* flanks, chloramphenicol resistance cassette and *fdxA* promoter [33]
pKfdxA	Complementation plasmid containing *cj0046* flanks, kanamycin resistance cassette and *fdxA* promoter [33]
pCASO27F	*cheY* (*cj1118c*) disruption plasmid, kan^R
pCASO28F	*cheW* (*cj0283c*) disruption plasmid, kan^R
pCASO54R	*cheA* (*cj0284c*) disruption plasmid, cat^R
pCASO69F	*cheV* (*cj0285c*) disruption plasmid, kan^R
pCASO59F	*cheY* complementation plasmid, cat^R
pCASO60F	*cheW* complementation plasmid, cat^R
pCASO58F	*cheA* complementation plasmid, kan^R
pCASO59^{D53A}	*cheY* ^{D53A} substitution mutant, cat^R
pCASO59D7A	*cheY* ^{D7A} substitution mutant, cat^R
pCASO72F	*cheV* complementation plasmid, cat^R
pCASO58Rec	Truncated *cheA* lacking C-terminal receiver domain complementation plasmid, kan^R
pCASO63	*fliN* complementation plasmid, kan^R
pCASO71F	*cheA-Y* complementation plasmid, cat^R
pMARKan9	Source of kanamycin resistance cassette [46]
pTopCat	Source of chloramphenicol resistance cassette

750 a. kan^R, kanamycin resistance; cat^R, chloramphenicol resistance

751

752 **LEGENDS TO FIGURES**

753

754 **Figure 1.** Architecture of the core CheV-A-W-Y chemotaxis system in *C. jejuni* compared to a
755 model Gram-negative (*E. coli* K-12) and Gram-positive (*B. subtilis* 168) organism.

756

757 **Figure 2.** Disrupting chemotaxis proteins does not impair flagella assembly. Brucella broth cultures
758 were grown overnight at 37°C in microaerobic conditions. Cell were mounted between a
759 microscope slide and coverslip and freshly prepared Ryu stain added adjacent to the coverslip. After
760 five minutes, areas where the Ryu stain had penetrated were photographed at ×100 magnification
761 using a Nikon Coolpix 4500 digital camera. Montage images and scale bars were prepared using
762 ImageJ. Scale bar = 2 microns.

763

764 **Figure 3.** Chemotaxis mutants show a significant reduction in chemotactic motility in soft agar. For
765 each chemotaxis mutant, the mutant strain was inoculated into 0.4% agar with the wild-type strain.
766 Halo formation was measured after 24 and 48 hours and halo area expressed as the percentage of
767 the wild-type halo for the same plate. Raw mean area of WT was 293.2 ± 15.52 and 1230 ± 63.69
768 mm^2 (24 and 48 hrs). Results are the mean from at least three biological replicates and error bars
769 show standard deviation. An asterisk denotes statistically significant results, based on a one-sample
770 *t*-test (comparison with wild-type) or a two-tailed Mann-Whitney test (*$p < 0.05$, **$p < 0.01$).

771

772 **Figure 4.** Chemotaxis mutants show a significant reduction in migration in an energy and redox
773 gradient. Tube taxis assays for each strain were monitored over 72 hours at 37°C and the dye front
774 measured after 24, 40, 48, 64 and 72 hours. Migration, calculated as a percentage of the wild-type
775 used in the same assay, is shown at 24, 48, and 72 hrs (a) and migration rate (mm hr^{-1}), compared to
776 WT is shown (b). Raw mean migration for WT was 8.198 ± 0.981, 19.77 ± 2.2, 25.58 ± 2.94, 40.48

777 ± 4.342, and 48.03 ± 5.09 mm (24, 40, 48, 64 and 72 hours). Results are the mean from at least four
778 biological replicates and error bars show standard deviation. Asterisks denote statistically
779 significant results, based on a one-sample *t*-test (comparison with wild-type) or a two-tailed Mann-
780 Whitney test (*$p < 0.05$, **$p < 0.01$)
781
782 **Figure 5.** The *cheY* mutants show a 'catherine wheel' swimming phenotype consisting of repeated
783 clockwise swimming. Following 6 – 7 hours growth at 37°C in microaerobic conditions, movies of
784 swimming cells (a, wild-type; b, *cheY*; c, *cheY* +*cheY*; d, *cheY* +*cheY*^{D53A}; e, *cheY* +*cheY*^{D7A}; f, *cheY*
785 +*cheA-Y*) were recorded at ×100 magnification using a light microscope and attached Nikon
786 camera. Individual cells were tracked using the Manual Tracking ImageJ plug-in and swimming
787 trajectories plotted using the Chemotaxis and Migration Tool (Ibidi).
788
789 **Figure 6.** Over-expressing a putative CheX homolog decreases swarming motility. a) Chemotactic
790 motility. Each strain was inoculated into 0.4% agar with the wild-type strain. Halo formation was
791 measured after 24 and 48 hours and halo area expressed as the percentage of the wild-type halo for
792 the same plate. Results are the mean from at least three biological replicates and error bars show
793 standard deviation. b) Tube Taxis. Assays were monitored over 72 hours at 37°C and the dye front
794 measured after 24, 48, and 72 hours. Migration was calculated as a percentage of the wild-type used
795 in the same assay. Results are the mean from at least three biological replicates and error bars show
796 standard deviation. c. Representative swarm plate and tube taxis assays showing the WT +*cheX*
797 phenotype. d. WT +*cheX* morphology shown using scanning electron microscopy and Ryu staining.
798 SEM scale bar = 1 micron, Ryu staining scale bar = 2 microns.
799
800 **Figure 7.** Chemotaxis is required for robust biofilm formation at the air-media interface. Static
801 cultures of each strain were grown in the presence of a sterile glass slide, as shown in the cartoon on

802 the right (37°C, microaerobic, 48 hrs). Glass slides were removed and stained with 1% crystal
803 violet. CV-stained biofilm was detected using a GenePix microarray scanner employing both 635
804 and 532 nm lasers. An asterisk shows the position of the air-media interface. Three independent
805 biological repeats are shown for each strain.
806
807 **Figure 8.** Chemotaxis model for *C. jejuni* (based on this and previous work) compared to *E. coli*
808 and *B. subtilis*. *C. jejuni* exemplifies a species-specific model of chemotaxis with similarities to the
809 Gram-positive model. White arrows show phosphate flow. Dotted white arrows suggest possible
810 phosphate flow. *H. pylori* CheZ (Cj0700) and ChePep (Cj1178c) homologs are shown as dashed
811 boxes.
812
813

814 **LEGENDS TO SUPPLEMENTARY INFORMATION**

815

816 **Figure S1**. Chemotaxis mutants do not show impaired growth in Brucella media in microaerobic
817 conditions. To measure growth, cultures grown overnight at 37°C in microaerobic conditions were
818 diluted to A600 = 0.05 in wells of a flat-bottom sterile 96 well-plate. Cultures were grown at 37°C
819 in 5% oxygen and 10% CO_2 and A600 was measured every 60 minutes for 24 hours using an
820 Omega plate reader attached to an atmospheric control unit (BMG Labtech).

821

822 **Figure S2**. RT-PCR analysis of chemotaxis gene expression in wild-type and mutant strains. Total
823 RNA was purified from various strains using the hot phenol method. cDNA was synthesised using
824 M-MuLV Reverse Transcriptase in the presence of murine RNase Inhibitor using a random primer
825 mix (OneTaq® RT-PCR Kit, NEB). Specific transcripts were amplified using One *Taq* DNA
826 polymerase using primers shown in supplementary Table 1. Primers specific for *rpoA* were used as
827 positive control primers and RT minus controls were included for each strain to control for
828 amplification from contaminating DNA. A) *cheV* transcript is absent in the *cheV* mutant, but not
829 *cheA* or *cheW* transcripts. B) *cheA* transcript is absent in the *cheA* mutant but *cheW* transcript is
830 present. C) *cheA-Y* transcript is present in the *cheA*+*cheA-Y* strain. D) CheY-complementation
831 strains express *cheY* transcripts. E) CheA-complementation strains express *cheA* transcripts.

832

833 **Figure S3**. Strains containing two copies of chemotaxis genes have altered swarming and migration
834 in taxis tubes. Swarm plate and tube taxis assay results from strains containing two copies of the
835 chemotaxis genes (original locus and *cj0046* complementation locus, constitutive *fdxA* promoter).
836 Results are the mean from at least three biological replicates and error bars show standard deviation.
837 An asterisk denotes statistically significant results, based on a one-sample *t*-test (comparison to
838 wild-type) or Mann-Whitney test (*$p < 0.05$).

839

840 **Figure S4**. *C. jejuni* CheY and CheA-Y share 58% similarity and contain the conserved acid pocket
841 and aspartic acid active site residues. A, multiple alignment of the Receiver Domain (PF00072)
842 seed sequences with NCTC11168 CheY, and the receiver domains of NCTC11168 CheA and CheV
843 (marked by an asterisk). Inset: model of NCTC11168 CheY threaded over CheY from *Thermotoga*
844 *maritima* (1TMY), active site aspartate residues are shown. B, Pairwise alignment of CheY and
845 CheA-Y from *C. jejuni* NCTC11168. Acid pocket and active site Asp residues are highlighted.

846

847 **Figure S5**. The *C. jejuni* CheA domain architecture is not unique to the Epsilon proteobacteria.
848 Stacked column charts showing the number of sequences from different phyla that share the domain
849 architecture of *C. jejuni* CheA as determined using the PfamAlyzer tool and NCBI taxomony.

850

851 **Figure S6**. The biofilm phenotype of the *che* mutants is linked to shedding of cells from the biofilm
852 and the ability to swim to the air-media interface. A) To assess cell shedding from the biofilm, the
853 A600 of each planktonic culture used to prepare slide biofilm assays was measured. Planktonic
854 cultures of at least three biological replicates were measured and error bars show standard
855 deviation. An asterisk denotes statistically significant results, based on a Mann-Whitney test (*$p <$
856 0.05, **$p < 0.01$, ***$p < 0.001$, ****$p < 0.0001$). B) Three biological replicates of the paralysed
857 flagella strain (*pflA*) in the slide biofilm assay. Freshly diluted cultures of Δ*pflA* (A600 = 0.05) were
858 incubated with a sterile microscope slide for 48 hours at 37°C in microaerobic conditions. Slides
859 were removed and strained with 1% crystal violet before scanning with a GenePixPro scanner.

860

861 **Supplementary Movie 1.** Swimming behaviour of the *C. jejuni cheY* mutant.

862

863 **Supplementary Movie 2.** Swimming behaviour of the *C. jejuni* WT +*cj0350* (*cheX*) strain.

864

865 **Table S1.** Oligonucleotide primers used in this study.

866

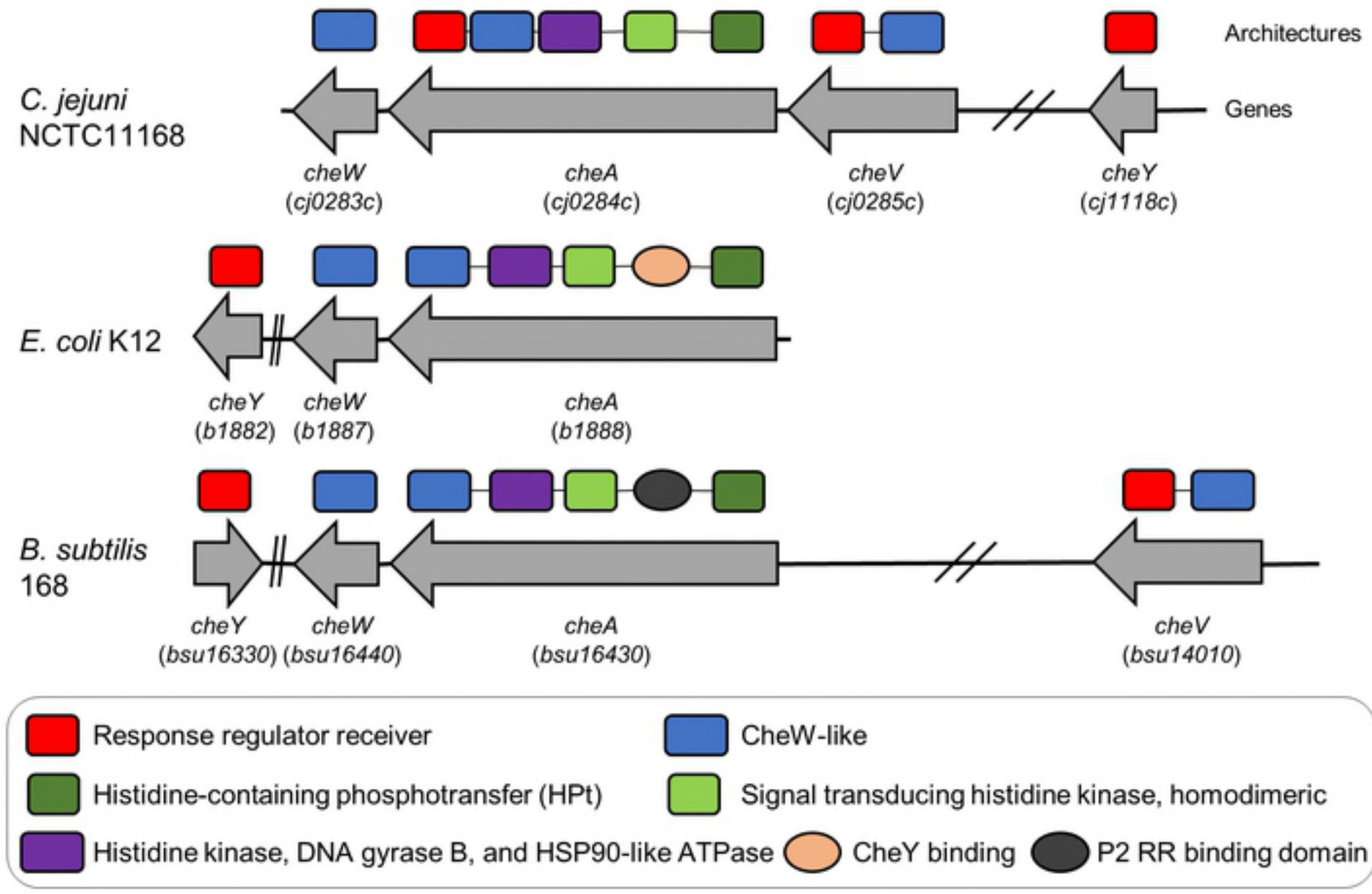

Reuter et al, Fig. 1

Figure 1

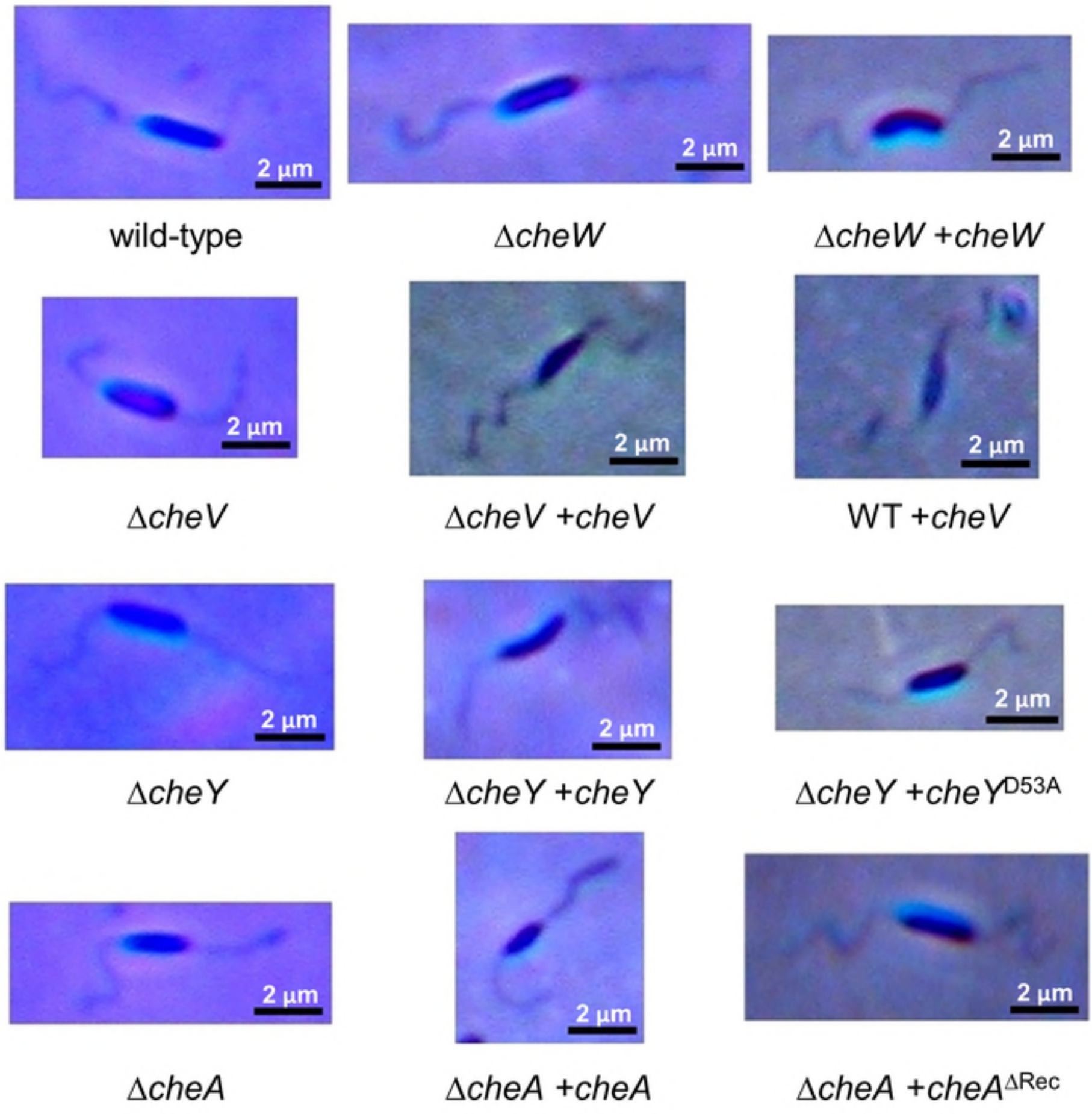

Reuter et al, Fig. 2

Figure 2

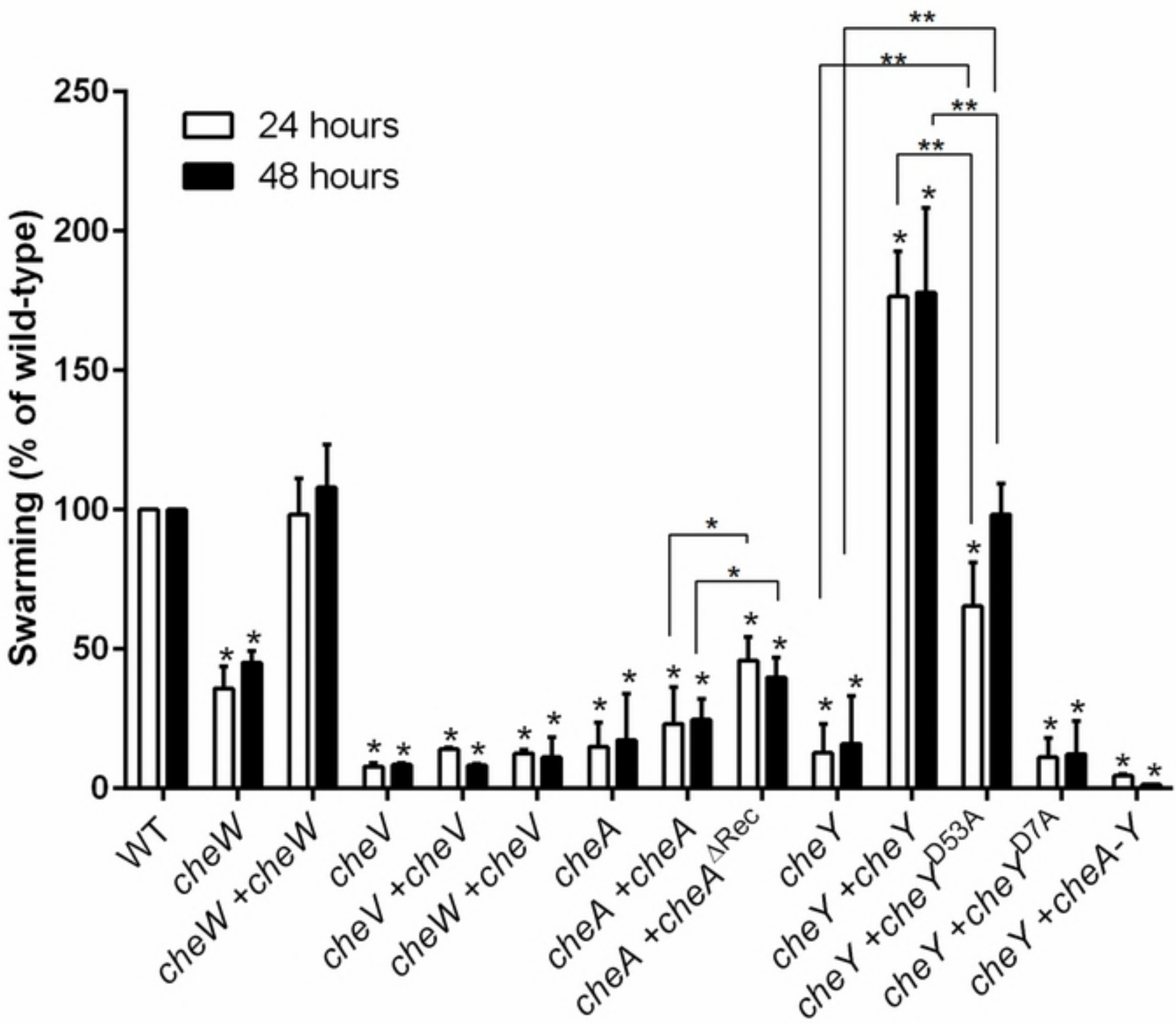

Reuter et al, Fig. 3

Figure 3

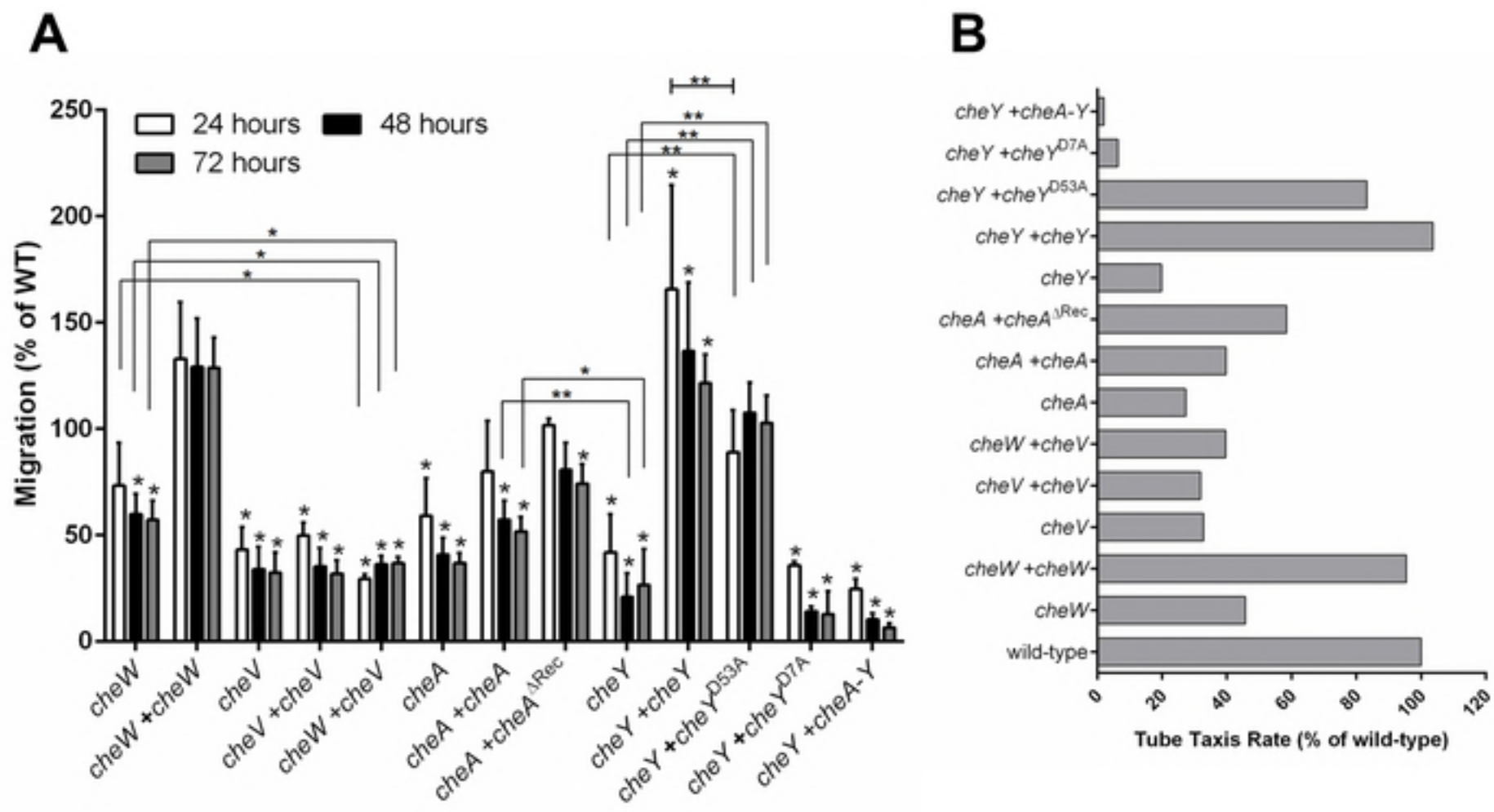

Reuter et al, Fig. 4

Figure 4

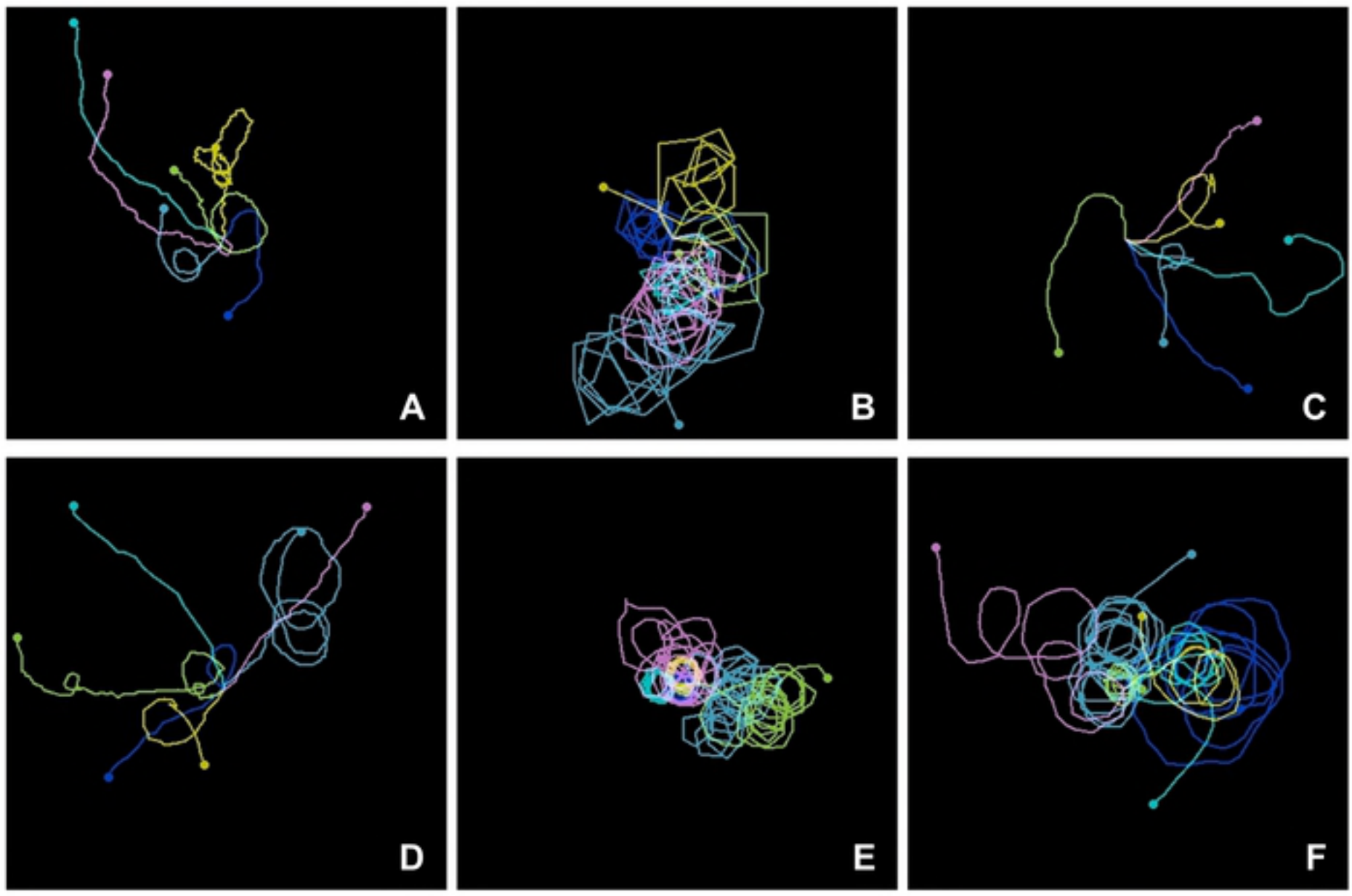

Reuter et al, Fig. 5

Figure 5

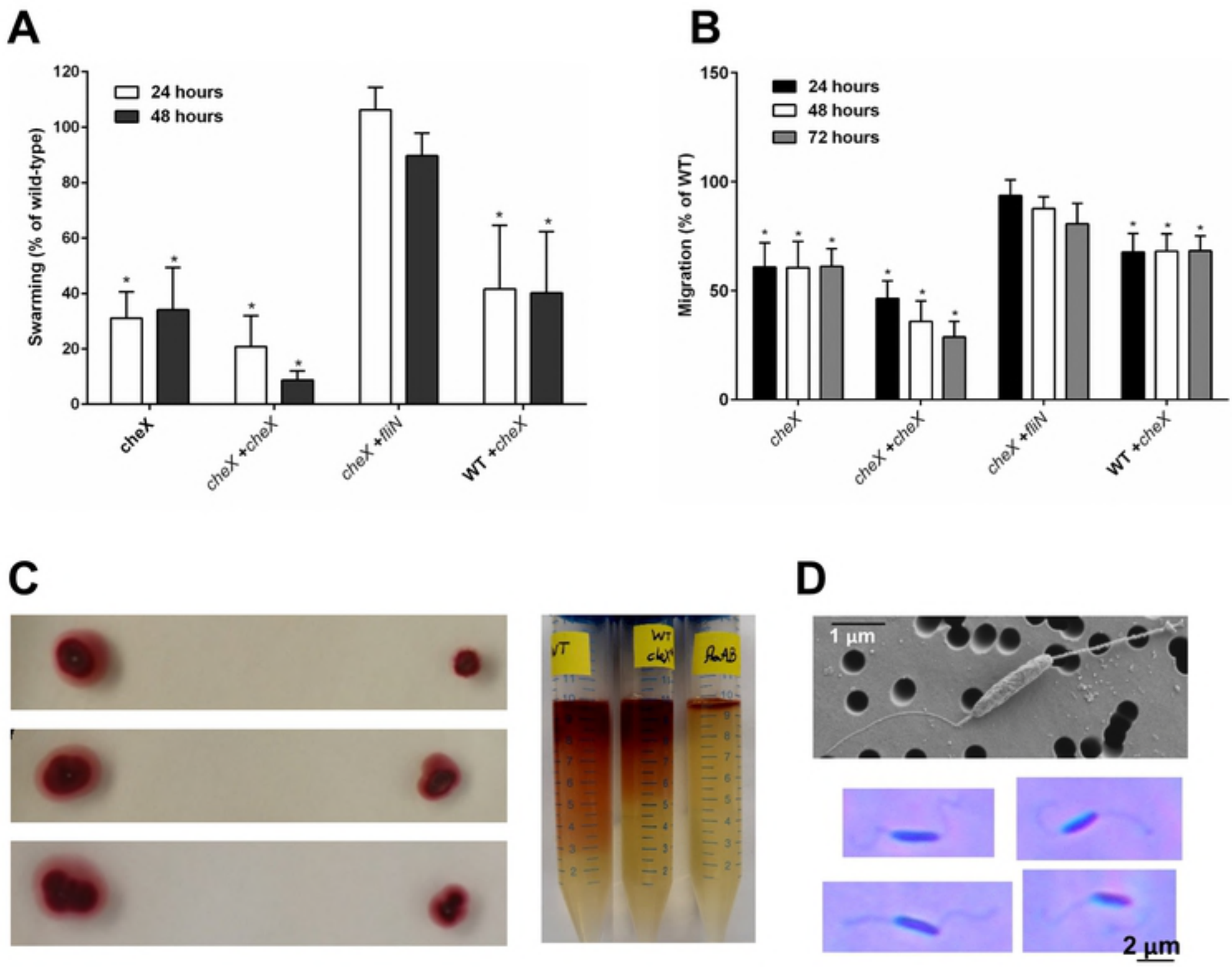

Reuter et al, Fig. 6

Figure 6

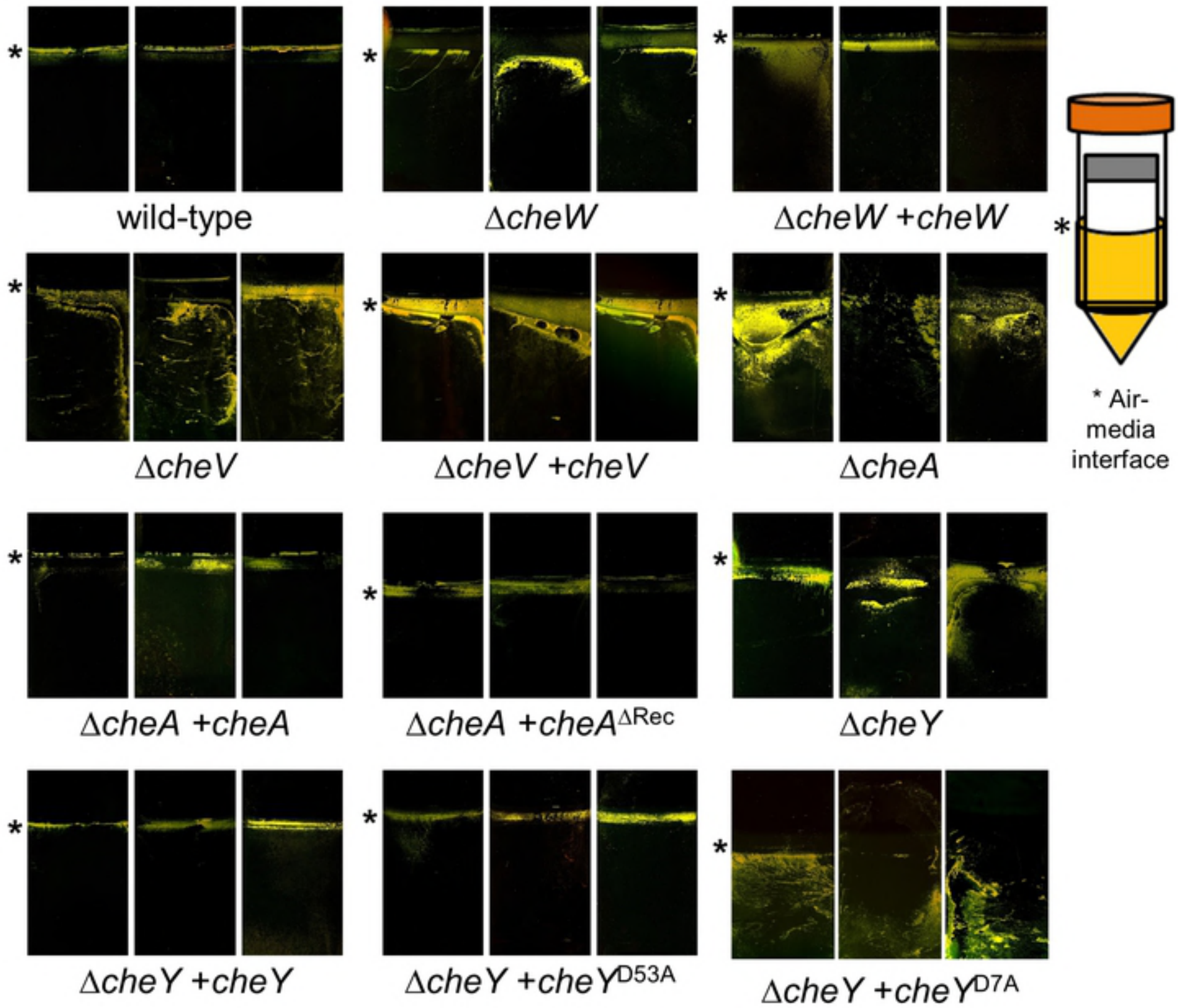

Reuter et al, Fig. 7

Figure 7

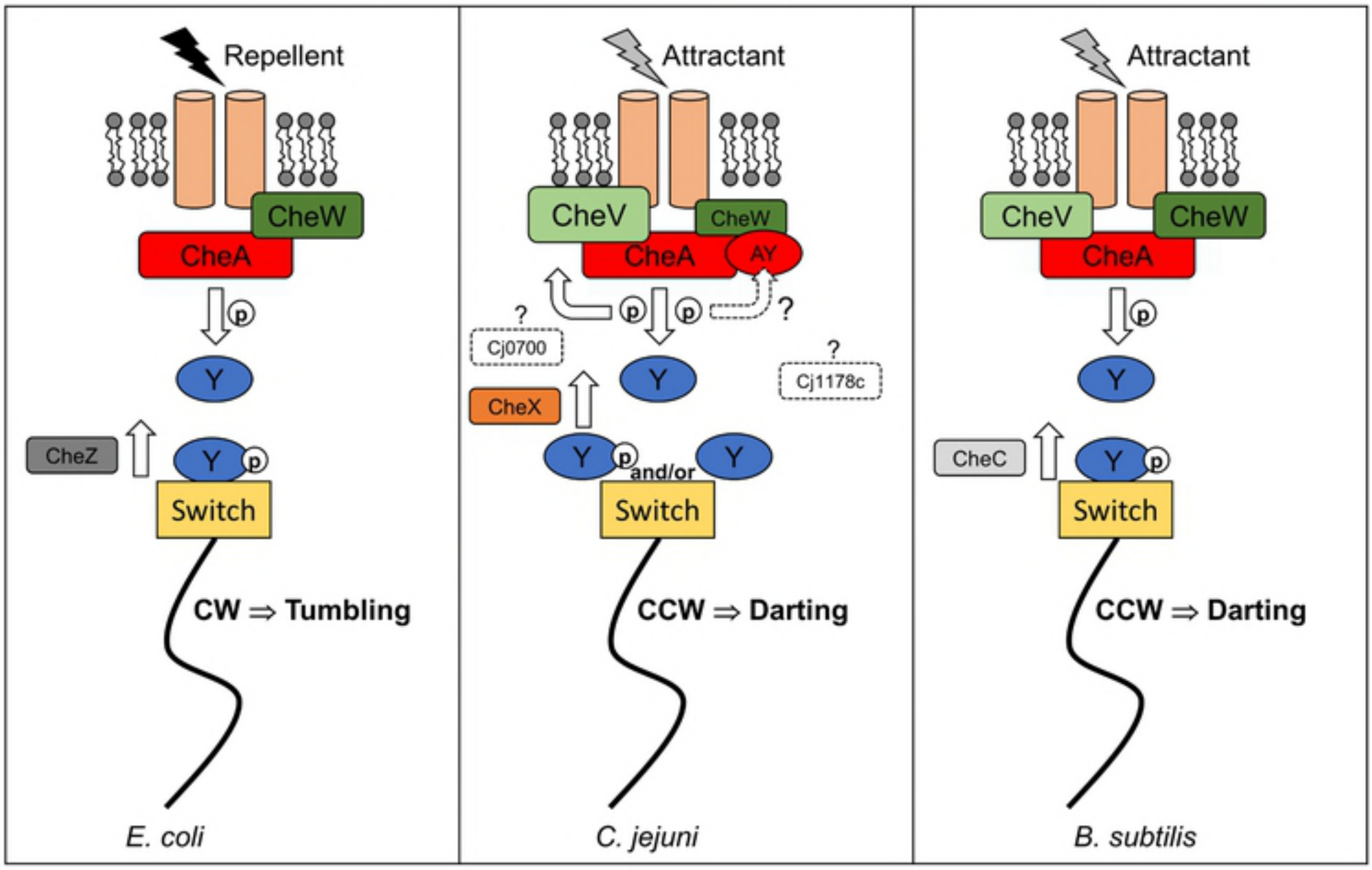

Reuter et al, Fig. 8

Figure 8